

Pilgrim: A thermal rate constant calculator and a chemical kinetics simulator

David Ferro-Costas^a, Donald G. Truhlar^b, Antonio Fernández-Ramos^{a,*}

^a*Centro Singular de Investigación en Química Biolóxica e Materiais Moleculares (CIQUS), Universidade de Santiago de Compostela, 15782 Santiago de Compostela, Spain*

^b*Department of Chemistry, University of Minnesota, 207 Pleasant Street SE, Minneapolis, Minnesota 55455-0431, USA*

Abstract

Pilgrim is a program written in Python and designed to use direct dynamics in the calculation of thermal rate constants of chemical reactions by the variational transition state theory (VTST), based on electronic structure calculations for the potential energy surface. *Pilgrim* can also simulate reaction mechanisms using kinetic Monte Carlo (KMC).

For reaction processes with many elementary steps, the rate constant of each of these steps can be calculated by means of conventional transition state theory (TST) or of the VTST. In the current version, *Pilgrim* can evaluate these thermal rates using the canonical version of reaction-path VTST, which requires the calculation of the minimum energy path (MEP) associated with each elementary step or transition structure. Multi-dimensional quantum effects can be incorporated through the small-curvature tunneling (SCT) approximation. These methodologies are available both for reactions involving a single structure of the reactants and the transition state and also for reactions involving flexible molecules with multiple conformations of the reactant and/or of the transition state. For systems with many conformers, the program can evaluate each of the elementary reaction rate constants by multipath canonical VTST or multi-structural VTST. Moreover, the reactant can be unimolecular or bimolecular.

Torsional anharmonicity can be incorporated through either the MSTor or the Q2DTor programs. Dual-level calculations are also available in *Pilgrim*: automatic high-level single-point energies can be used to correct the energy of reactants, transition states, products, and MEP points using the interpolated single-point energies (ISPE) algorithm.

When the rate constants of all the chemical processes of interest are known, by means of their calculation using *Pilgrim* or alternatively through analytical fits to the rate constants as functions of temperature, it is possible to simulate a multistep mechanism under specified laboratory conditions using KMC. This algorithm allows performing a kinetic simulation to monitor the evolution of each chemical species with time and obtain the product yields.

Keywords: transition state theory, variational transition state theory, multipath variational transition state theory, minimum energy path, multidimensional tunneling, multiple conformations, dual-level direct-dynamics calculations, kinetic Monte Carlo, reaction mechanisms, chemical kinetics

*Corresponding author, E-mail address: qf.ramos@usc.es
Preprint submitted to *Computer Physics Communications*

PROGRAM SUMMARY

Program Title: *Pilgrim*

Licensing provisions: MIT

No. of lines in distributed program, including test data, etc.:

Computer code: 21088 lines;

Computer code + tests: 2356172 lines;

Distribution format: tar.gz and zip

Program obtainable at: <https://github.com/cathedralpkg/pilgrim/releases>

Programming language: Python 3

Operating system: Linux or Unix

Computer: No computer-specific

Nature of problem: Calculation of thermal rate constants for bimolecular and unimolecular chemical reactions and simulation of reaction mechanisms

Solution method: The program uses variational transition state theory to calculate thermal rate constants and kinetic Monte Carlo to simulate reaction mechanisms.

Restrictions and unusual features: The program cannot treat reactions without saddle points. Unimolecular reactions are calculated only in the high-pressure limit. Direct dynamics calculations with *Pilgrim* require an electronic structure package to be supplied by the user; currently, *Pilgrim* supports the *Gaussian* [1–3] and *Orca* [4] electronic structure packages. *Pilgrim* has an especially powerful suite of options for handling torsional anharmonicity and multistructural effects.

1. Introduction

Pilgrim is a program for direct dynamics calculations of chemical reaction rates by variational transition state theory (VTST) [5–11] including transmission coefficients to account for multidimensional tunneling. In direct dynamics, instead of using an analytic potential energy function, all required energies, forces, and force constants (a force constant is an element of the Hessian matrix) needed for each step of dynamics are obtained directly from electronic structure calculations [12–14], and for this purpose *Pilgrim* interfaces with an electronic structure program supplied by the user. VTST is an efficient method for the calculation of thermal rate constants of chemical reactions, and its accuracy has been validated both by applications to accurate quantum dynamics for small systems and by applications to many larger systems for which experimental rate constants and/or kinetic isotope effects are available [15–17].

The success of VTST is due to the fact that, as compared to conventional [18] transition state theory (TST), it improves the treatment of two key aspects of TST. Those two aspects are [19] (1) the no-recrossing assumption and (2) the treatment of quantum effects. The no-recrossing assumption considers that when the system passes through the transition state (which is a hyper-surface in phase space dividing reactants from products) toward products, it always proceeds to products without recrossing the dividing surface and without having crossed it previously. VTST improves over conventional TST for this aspect by optimizing the location of the transition state dividing surface; the optimized dividing surface is called the variational transition state. The second aspect is that quantum effects are important not only for the partition functions of bound modes but also for the transmission coefficient, which should include quantum effects on the reaction-coordinate motion. Although conventional TST without a transmission coefficient includes the former (by quantizing the vibrations of the reactant and the vibrational degrees of freedom transverse to the reaction coordinate at the transition state), it does not have adequate methods for including tunneling in the reaction-coordinate motion. In particular, although tunneling is sometimes added to conventional transition state theory by a transmission coefficient [20–23], it is hard to do this consistently in the general case, because the correct way to calculate tunneling is to use the vibrationally adiabatic potential [24], and since this does not necessarily have its maximum at the saddle point, one needs to add tunneling to variational transition state theory to get a consistent result [25]. In contrast, VTST includes a multiplicative transmission coefficient κ that accounts for multidimensional tunneling and nonclassical reflection by a multidimensional dynamics calculation that uses an effective barrier whose determination involves all degrees of freedom.

The present article is limited to presenting the *Pilgrim* computer program, and space does not permit reviewing the details of all the methods and other aspects of aspects of VTST. The reader may consult the reviews already given for general background [5, 7–9] and for full details of the methods [6, 10, 11]. In many cases we also give the original references for methods as part of the discussion in the rest of this article.

When vibrations of the reactant and the vibrational degrees of freedom transverse to the reaction coordinate at the transition state are quantized, the calculation is called quasiclassical. All calculations carried out by *Pilgrim* are quasiclassical. *Pilgrim* also assumes that the Born-Oppenheimer approximation is valid so that the potential energy V for nuclear motion is given by the electronic energy (which, by convention, includes nuclear repulsion) at the given geometry. *Pilgrim* also assumes that nonreactive energy-transfer processes are faster than chemical reaction steps so that reactants maintain their internal states in thermal equilibrium even while the reaction proceeds.

The quantum mechanical thermal rate constant at a given temperature T for a gas-phase elementary process can be written as:

$$k(T) = \gamma(T) \cdot k^\ddagger(T) \quad (1)$$

where $k^\ddagger(T)$ is the rate constant calculated by quasiclassical conventional TST.¹ The complete (or overall) transmission coefficient is a product of two factors:

$$\gamma(T) = \Gamma(T) \cdot \kappa(T) \quad (2)$$

where $\Gamma(T)$ accounts for recrossing effects and $\kappa(T)$ for quantum effects on the reaction coordinate.² Note that $\Gamma(T) \leq 1$ and that $\kappa(T)$ is usually ≥ 1 . A practical way to estimate these two coefficients is to use VTST since it effectively evaluates $\Gamma(T)$, by finding a dividing surface with less recrossing than the conventional transition state, and it evaluates $\kappa(T)$ by using semiclassical methods.³

Pilgrim calculates $\Gamma(T)$ as the ratio between canonical variational transition state theory (CVT) [26, 27] and conventional TST [18] thermal rate constants,

$$\Gamma^{\text{CVT}}(T) = \frac{k^{\text{CVT}}(T)}{k^\ddagger(T)} \quad (3)$$

whereas the tunneling transmission coefficient $\kappa^{\text{CVT/SCT}}$ is calculated using the semiclassical small-curvature tunneling (SCT) approximation [28–30]. Therefore, the thermal rate constant of Eq. (1) is given by:

$$k^{\text{CVT/SCT}} = \gamma^{\text{CVT/SCT}} \cdot k^\ddagger = \kappa^{\text{CVT/SCT}} \cdot \Gamma^{\text{CVT}} \cdot k^\ddagger \quad (4)$$

In Eq. (4) we have omitted the temperature dependence for simplicity. The factor $\kappa^{\text{CVT/SCT}}$ is called the tunneling transmission coefficient, Γ^{CVT} is called the recrossing transmission coefficient, and $\gamma^{\text{CVT/SCT}}$ is the (overall) transmission coefficient. The deviation of Γ^{CVT} from unity is called a variational effect. The calculation of k^\ddagger involves optimization of the reactant and conventional transition state structures (the latter are saddle points) and the calculation of their energies and partition functions.⁴ The calculation of the transmission coefficients involves calculating a minimum-energy path (MEP) through each considered saddle point and the calculation of energies and partition functions along each path.

Pilgrim can perform TST and CVT/SCT for elementary reactions having species with several conformational isomers of the reactant(s) and/or transition state. These conformers, which are usually rotamers (i.e., conformers connected by torsions, which are also called internal rotations), are called structures. The program can take into account the contributions of all the conformers to the thermal rate constant. If all reactant and transition state structures are included

¹Hereafter, the symbol \ddagger denotes conventional TST or the conventional transition state, which is a dividing surface that passes through the saddle point that corresponds to the highest-energy point on the lowest-energy path from reactants to products.

²Technically, since we use a multidimensional tunneling calculation, it accounts not only for quantum effects on the reaction coordinate but also for the coupling of the quantum mechanical reaction coordinate to the other coordinates.

³*Pilgrim* always treats quantum effects on the reaction coordinate motion semiclassically (by a multidimensional extension of the Wentzel-Kramers-Brillouin approximation), but it is still correct to refer to them as quantum effects.

⁴The optimizations are done externally as described below.

Table 1: Required input files for the methods implemented in *Pilgrim*. MS and MP versions of the rate constant require the same input files.

Input files	Methods		
	(MS)-TST	(MS)-CVT,(MS)-CVT/SCT	KMC
<i>pif.temp</i>	×	×	×
<i>pif.chem</i>	×	×	×
<i>pif.struc</i>	×	×	
<i>pif.path</i>		×	
<i>pif.calcs</i>		×	
<i>pif.kmc</i>			×

in the partition functions, and if variational and quantum effects are calculated using only the reaction path associated with the transition state with the lowest energy or lowest free energy, the calculated rate constant is called multi-structural CVT/SCT (MS-CVT/SCT) [31, 32]. When – at greater cost – variational and quantum effects are calculated taking into account the reaction paths associated with multiple transition state structures, the calculated thermal rate constant is called multipath CVT/SCT (MP-CVT/SCT) [33, 34]. *Pilgrim* can also incorporate torsional anharmonicity, calculated by the Q2DTor [35] program or the MSTor [36, 37] program, to evaluate these thermal rate constants. Moreover, *Pilgrim* also allows handling several elementary reactions at the same time as part of a given reaction mechanism, which can be simulated by means of kinetic Monte Carlo (KMC) [38, 39].

A schematic structure of the main features of *Pilgrim* is shown in Figure 1. The basic instruction for executing *Pilgrim* is:

```
pilgrim.py --option
```

where `--option` is indicated in red in Figure 1. All of the input files can be generated or modified by typing:

```
pilgrim.py --input
```

Figure 1 shows three alternative routes to the product yields. The solid arrows indicate the route to perform a full MP-CVT/SCT calculation, the dotted path marks an alternative route where only TST or MS-TST rate constants are requested, and the dashed path indicates a direct route to perform KMC calculations using reaction mechanisms for which the rate constants of all the elementary steps are already available from an analytical expression. All three routes are discussed below. The number of input files required depends on the type of calculation requested (see Table 1). A full account of the capabilities of *Pilgrim*, the keywords, and several worked examples are given in the manual of the program; however, here we want to establish a direct connection between the theory behind VTST and KMC methods and the input/output of the program.

In order to illustrate some of the rate constant features of *Pilgrim*, for instance the calculation of MS-TST and MP-CVT/SCT thermal rate constants, Section 2 considers the following elementary reactions:

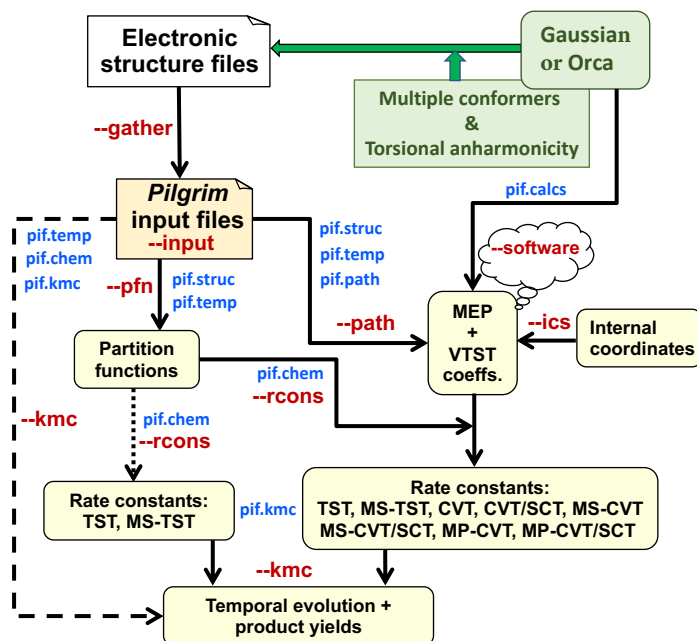


Figure 1: Flow diagram showing the main options of *Pilgrim* (in red), the input files needed in each case (in blue), and the output provided by the program (yellow rectangles). The `--software` option is used to specify the electronic structure software. *Gaussian* is the default but *Orca* can be specified with this option.



Selected Pilgrim outputs are collected in A. Section 3 considers the decomposition reactions of the 1-propanol radical of Ref. 40 (Table 2) with the purpose of exemplify the KMC simulations. Selected Pilgrim outputs are presented in E.

2. Study of elementary reactions using *Pilgrim*

A chemical reaction is considered elementary if one or a pair of reactants lead to a particular chemical product or pair of products in a single reaction step. The elementary reaction may be barrierless or it may have a saddle point. Currently, *Pilgrim* can only carry out direct dynamics for elementary reactions that have a saddle point. For barrierless reactions we recommend PolyRate [41]. Notice that despite this limitation, *Pilgrim* can perform the KMC calculations incorporating barrierless reactions if the rate constants are provided by the user, as discussed in Section 3 of this article. The program can also handle cases where the single step leads to multi-structural products (a given chemical species or pair of species where one or both of the species has multiple conformations).

Table 2: Reactions considered to test the KMC algorithm of *Pilgrim*.

Name	Reaction
R1	$\text{CH}_3\text{CH}_2\text{CH}_2\text{O}\cdot \rightarrow \text{CH}_2\text{O} + \cdot\text{CH}_2\text{CH}_3$
R2	$\text{CH}_3\text{CH}_2\text{C}\cdot\text{HOH} \rightarrow \text{HOCHCH}_2 + \cdot\text{CH}_3$
R3	$\text{CH}_3\text{CH}_2\text{C}\cdot\text{HOH} \rightarrow \text{H}\cdot + \text{OCHCH}_2\text{CH}_3$
R4c	$\text{CH}_3\text{CH}_2\text{C}\cdot\text{HOH} \rightarrow \text{H}\cdot + \textit{cis}\text{-HOCHCHCH}_3$
R4t	$\text{CH}_3\text{CH}_2\text{C}\cdot\text{HOH} \rightarrow \text{H}\cdot + \textit{trans}\text{-HOCHCHCH}_3$
R5	$\text{CH}_3\text{CH}_2\text{CH}_2\text{O}\cdot \rightarrow \text{H}\cdot + \text{OCHCH}_2\text{CH}_3$
R6	$\cdot\text{CH}_2\text{CH}_2\text{CH}_2\text{OH} \rightarrow \cdot\text{CH}_2\text{OH} + \text{CH}_2\text{CH}_2$
R7	$\text{CH}_3\text{CH}_2\text{CH}_2\text{O}\cdot \rightleftharpoons \cdot\text{CH}_2\text{CH}_2\text{CH}_2\text{OH}$
R8c	$\text{CH}_3\text{C}\cdot\text{HCH}_2\text{OH} \rightarrow \text{H}\cdot + \textit{cis}\text{-HOCHCHCH}_3$
R8t	$\text{CH}_3\text{C}\cdot\text{HCH}_2\text{OH} \rightarrow \text{H}\cdot + \textit{trans}\text{-HOCHCHCH}_3$
R9	$\text{CH}_3\text{CH}_2\text{CH}_2\text{O}\cdot \rightleftharpoons \text{CH}_3\text{CH}_2\text{C}\cdot\text{HOH}$
R10	$\text{CH}_3\text{CH}_2\text{CH}_2\text{O}\cdot \rightleftharpoons \text{CH}_3\text{C}\cdot\text{HCH}_2\text{OH}$
R11	$\text{CH}_3\text{C}\cdot\text{HCH}_2\text{OH} \rightarrow \text{H}\cdot + \text{OHCH}_2\text{CHCH}_2$
R12	$\text{CH}_3\text{CH}_2\text{C}\cdot\text{HOH} \rightleftharpoons \text{CH}_3\text{C}\cdot\text{HCH}_2\text{OH}$
R13	$\text{CH}_3\text{C}\cdot\text{HCH}_2\text{OH} \rightleftharpoons \cdot\text{CH}_2\text{CH}_2\text{CH}_2\text{OH}$
R14	$\text{CH}_3\text{CH}_2\text{C}\cdot\text{HOH} \rightleftharpoons \cdot\text{CH}_2\text{CH}_2\text{CH}_2\text{OH}$
R15	$\cdot\text{CH}_2\text{CH}_2\text{CH}_2\text{OH} \rightarrow \text{H}\cdot + \text{HOCH}_2\text{CHCH}_2$
R16	$\text{CH}_3\text{C}\cdot\text{HCH}_2\text{OH} \rightarrow \cdot\text{OH} + \text{CH}_2\text{CHCH}_3$

This section describes the setup of the input files and the output provided by *Pilgrim*, as well as the theory to calculate the MS-TST and MP-CVT/SCT thermal rate constants for reactions **R1h** and **R1d**. *Pilgrim* performs direct-dynamics calculations [12–14], that is, the energies, forces, and force constants on the potential energy surface (PES) are calculated ‘on the fly’ by an external electronic structure software package, which is denoted as the ESSO. *Pilgrim* requires the user to supply the ESSO; currently, it supports only the *Gaussian* [1–3] and *Orca* [4] electronic structure packages.

Notice that other ESSO can be also incorporated to *Pilgrim* by creating a new Python module inside the `modpilgrim` library, similar to `itf_orca.py` (for *Orca*) and `itf_gau.py` (for *Gaussian*) modules. These Python functions read the energy, gradient, and Hessian of *Orca* or *Gaussian*, and users can adapt *Pilgrim* to use another electronic structure program by writing a similar script for that program. Once created, the user just needs to include this new module in the `dsoft` dictionary defined inside the `itf.py` module. In this way one can use other electronic structure programs.

For the examples considered here, all the electronic structure calculations were performed at the HF/STO-3G level [42]. This is too low of a level to be quantitatively useful for practical rate calculations, but we chose a low level to make the illustrative calculations inexpensive in case a user wants to use them as a learning experience.

2.1. Preliminaries

The location of the ESSO executable(s) must be specified in the `.bashrc` file. For instance,

```
# Path to $Gaussian$ executables
```

```
export GauExe="/home/programs/g09/g09"  
export GauFchk="/home/programs/g09/formchk"  
  
# Path to $Orca$ executable  
export OrcaExe="/home/programs/orca_4_0_1_2/orca"
```

where `GauExe` and `GauFchk` are the variables that export the routes of the *Gaussian* executable and *formchk* utility, respectively. For *Orca* users, the route of the executable is exported through `OrcaExe`.

To start the calculation of the thermal rate constants, *Pilgrim* requires the optimized structures of the stationary points involved in the reaction. For instance, to study reaction **R1h**, we create a working directory called `EtOHabs/`. Inside this directory, the subdirectory `UDATA/` should be created. Notice that `UDATA/` should contain the electronic structure files (ESFILs) with the stationary points (minima and transition structures) of all species of all reactions that the user wishes to study.⁵ Every ESFIL should contain the optimized geometry of a structure and the corresponding Hessian matrix.⁶

For a species with more than one conformer, all the ESFILs should be included in the same directory inside `UDATA/`. The name given to this directory is used by *Pilgrim* as the label that identifies that species. In the case of species without conformers the ESFIL may hang directly from `UDATA/`. In that case, the label that identifies the species is the name of the ESFIL without its extension.

Hereafter, those labels are called by the generic name of `sname`. The names of the ESFILs and of the `sname` (in blue) are displayed in Figure 2. The generic label `tsname` designates a `sname` structure that is a transition structure. For reaction **R1h**, ethanol, the hydrogen atom, the ethoxy radical and the hydrogen molecule were labeled as `CH3CH2OH`, `H`, `CH3CH2O`, and `H2`, respectively. The transition state for the hydrogen abstraction from the hydroxyl group was labeled as `TSoh`.

The ethanol molecule has three conformations, one conformation with the methyl and hydroxyl groups in *anti* and two conformations with these two groups in *gauche*. The two *gauche* conformers are conformational enantiomers with the same electronic structure properties; therefore only one of the two needs to be specified. Similarly, the transition state has three conformations, and the two *gauche* conformations are conformational enantiomers. In the case of ethanol the ESFILs of the two structures (one *anti* and one *gauche*) are placed in the `CH3CH2OH/` directory, whereas those of the transition state go inside `TSoh/`.

When *Pilgrim* is executed with option `--gather`,

```
pilgrim.py --gather
```

⁵Notice that a transition structure is a saddle point between reactants and products, and it should not be confused with a transition state, which is a hypersurface in phase space separating reactants from products. A transition state may be associated with zero, one, or multiple transition structures, but *Pilgrim* is not designed to handle the case with zero transition structures.

⁶A structure may be a stable structure, which is a local or global minimum on the potential energy surface, or it may be a transition structure. A chemical species may be a stable species or a transition state; it is associated with one or more stable structures or one or more transition structures, respectively. Structures that are connected to other structures of the same species by internal rotation are called conformers or rotamers.

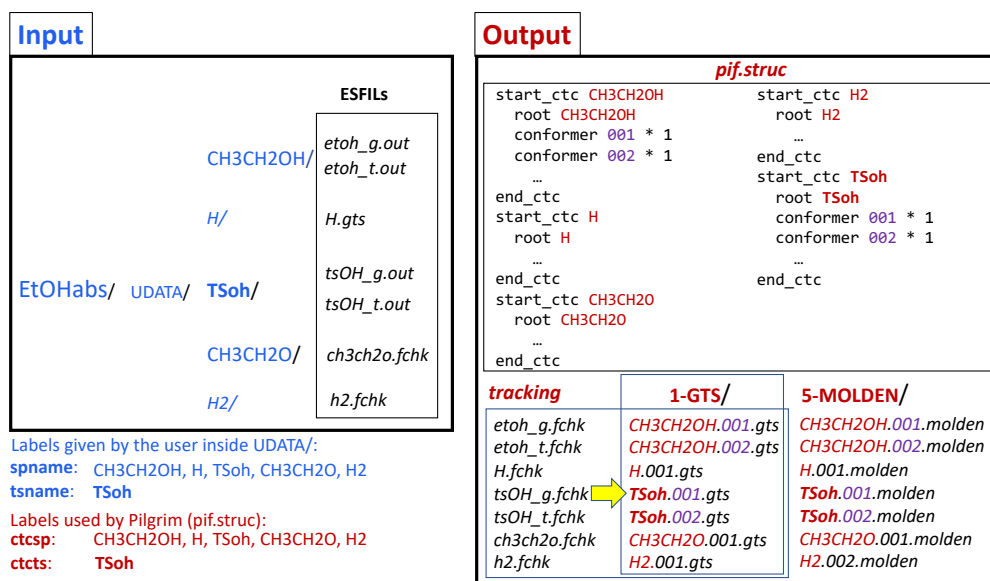


Figure 2: Structure of the files for reaction R1h after executing the `--gather` option.

the program generates two files and two directories. The two directories are: 1-GTS/ and 5-MOLDEN/. The former contains the same information as that in the ESFILs placed in UDATA/, but with a uniform format more suitable for *Pilgrim* calculations. The files inside 1-GTS/ are named using the format *sname.idx.gts*, where *idx* is an index that runs from 001 to the number of conformers for the species with label *sname*. The conformers are sorted by *Pilgrim* in the 1-GTS/ directory by increasing energy.

At this stage we need to introduce the concept of a cluster of torsional conformers (CTC). For a given reaction, we first find all the structures of the transition state. If all the structures of the reactants can be interconverted among one another by internal rotations, and all the structures of the transition state can be converted into one another by internal rotation, then a reaction is said to have one CTC. If however, the structures divide into N_T groups that cannot be interconverted among one another by internal rotation, then that reaction has N_T CTCs. The final rate must be summed over contributions from each CTC. Within a given CTC, there may be multiple conformers of the reactant and/or of the transition state, and these should all be included by MS-CVT/SCT or MP-CVT/SCT.

The program creates two files: *tracking* and *pif.struc*. The former correlates the files of UDATA/ with the files in 1-GTS/ (see Figure 2); the latter contains information about each of the stationary points given inside UDATA/. The *pif.struc* file contains CTC blocks beginning with *start_ctc* and ending with *end_ctc*. The generic names *ctcsp* and *ctcts* are used instead of *sname* and *tsname*, respectively. The former pair is used to refer to molecules which may be affected by isotopic substitutions, whereas the latter pair is isotope independent. Thus, for the **R1d** reaction, new *ctcsp* and *ctcts* blocks can be defined using the information of the root species (*sname* and *tsname*).

2.2. Input for conventional TST calculations

With the exception of the *pif.struc* file, which was created at a previous stage, the rest of *Pilgrim* input files can be generated through the interactive menu (Listing A.1), accessible via:

```
pilgrim.py --input
```

Depending on the file to be addressed, there are various options available, and they can be chosen as follows:

```
> $cmd $var [$values]
```

where (>) is the prompt.

For reaction **R1h**, both ethanol and the transition state have two conformational enantiomers (the two *gauche* structures). The list of all species can be accessed inside the menu by typing:

```
> ls struc
```

leading to the output of Listing A.2. It indicates that for ethanol, labeled as CH3CH2OH, there are a total of two conformations in the same CTC, although there should be three of them because one of the structures has a conformational isomer. The reason is that the *gauche* conformer is endowed with a weight of 1. In general, inside a CTC block the user should include all the distinguishable structures with their conformational weight but excluding conformational enantiomers. The conformational weight is two for a structure with a conformational enantiomer and is unity otherwise. We denote the total number of structures of a minimum as N_c and, in the case of a saddle points as J_c^\ddagger . Therefore the total number of distinguishable conformers of a given minimum is

$$N_c = \sum_n w_n \quad (5)$$

and of a saddle point

$$J_c^\ddagger = \sum_j w_j^\ddagger \quad (6)$$

where w_n and w_j^\ddagger are the conformational weights of the n -th and the j -th conformer of the corresponding minimum and transition structure, respectively (see Listing A.3).

Table 1 provides a list of the input files that are needed in order to calculate the thermal rate constants by a given method. The MS-TST calculations operate with the *pif.struc*, *pif.temp*, and *pif.chem* input files. The add command inside the input menu can be used to create (if it does not exist) the file associated with the variable listed in Listing A.1. A working temperature of 298.15 K for the calculation of the rate constants can be specified with the command

```
> add temp 298.15
```

which creates the *pif.temp* file with the corresponding temperature. The chemical reaction is specified with:

```
> add chem R1h : CH3CH2OH+H --> TSoh --> CH3CH2O + H2
```

which creates the file *pif.chem*. No further input files are required for the calculation of MS-TST rate constants.

2.2.1. Adding isotopically substituted reactions

In addition to reaction **R1h**, we want to study reaction **R1d**. In that case the *pif.struc* needs to be modified (using the `--input` option) to accommodate the isotopically substituted species. In *Pilgrim* the isotopically substituted species are created from existing root species. Thus, CH3CH2OD can be created from CH3CH2OH by typing:

```
> mod struc CH3CH2OH
>> copywith D(9) as CH3CH2OD
```

The first line enters the CH3CH2OH block inside *pif.struc* and the second line copies that structure as a new structure (a `ctcsp`) called CH3CH2OD where atom number 9 has been substituted by a deuterium. In the same manner:

```
> mod struc H
>> copywith D(1) as D
> mod struc H2
>> copywith D(all_H) as D2
> mod struc TSoh
>> copywith D(9,10) as TSod
```

All species are given in Listing A.4, and the resulting *pif.struc* file is schematized in Figure 3. After those modifications, reaction **R1d** should be incorporated into *pif.chem* in the same manner as reaction **R1h**.

```
> add chem R1d : CH3CH2OD+D --> TSod --> CH3CH2O + D2
```

2.3. Partition functions

With the information collected from the ESFILS, *Pilgrim* can calculate the total partition function of each species, in which the translational and electronic partition functions (Q_{trans} and Q_{el} , respectively) are assumed to be separable from the rovibrational partition function, Q_{rv}^{X} :

$$Q^{\text{X}} = Q_{\text{trans}} Q_{\text{el}} Q_{\text{rv}}^{\text{X}} \quad (7)$$

where X indicates the approximation to evaluate the rovibrational partition function. The translational partition function is defined as

$$Q_{\text{trans}} = \Phi_{\text{trans}} V^{\circ} = \left(\frac{M}{2\pi\hbar^2\beta} \right)^{3/2} V^{\circ} \quad (8)$$

where M is the mass of the system, V° is the volume per particle in the standard state, \hbar is the Planck's constant divided by 2π , and $\beta = (k_{\text{B}}T)^{-1}$, with k_{B} being the Boltzmann constant, and T being the temperature.

```

start_isomass
D = 2.0141
end_isomass
start_ctc CH3CH2OH
root CH3CH2OH
conformer 001 * 2
conformer 002 * 1
...
end_ctc
...
start_ctc TSoh
root TSoh
conformer 001 * 2
conformer 002 * 1
...
end_ctc
... (continues in
the next column)

start_ctc CH3CH2OD
root CH3CH2OH
conformer 001 * 2
conformer 002 * 1
...
iso D(9)
end_ctc
start_ctc TSod
root TSoh
conformer 001 * 2
conformer 002 * 1
...
iso D(9,10)
end_ctc
start_ctc D
root H
...
iso D(1)
end_ctc
start_ctc D2
root H2
...
iso D(all_H)
end_ctc

```

Section added to *pif.struc* after isotopic substitutions
 New *ctcsp* labels : CH3CH2OD, D, D2 and TSod
 New *ctcts* label: TSod

New *ctcts* label
 Root species from which TSod was created

Mass of atoms 9 and 10 changed to the mass
 labelled as D in start_isomass

Figure 3: Extract of the *pif.struc* file after including the isotopically substituted species. The TSod transition state was highlighted with explanation of some of the keywords associated with isotopes.

The electronic partition function is given by

$$Q_{\text{el}} = g_0 + \sum_{i=1} g_i e^{-\beta \epsilon_i} \quad (9)$$

where g_0 is the degeneracy of the electronic ground state, and g_i and ϵ_i are the degeneracy and relative energy of the i -th electronic excited state. Equation 9 includes all electronic states, but by default the file *pif.struc* generated by *Pilgrim* only includes the ground electronic state obtained from the electronic structure calculations. However, low-lying electronic excited states can be included in the *pif.struc* file with the `elstate` keyword.

In *Pilgrim*, if one uses the single-structure rigid-rotor (RR) harmonic-oscillator (HO) approximation or the single-structure rigid rotor quasiharmonic (QH) approximation (X = RRHO or RRQH), the rovibrational partition function is considered to be a product of a rotational factor and a vibrational factor. These two approximations are implemented for the one-structure (one conformation) or the multi-structural (multiple conformations) cases.

For one structure, the rovibrational RRHO partition function is given by:

$$Q_{\text{rv}}^{\text{RRHO}} = Q_{\text{rot}} Q^{\text{HO}} \quad (10)$$

The rotational partition function for nonlinear molecules is given by

$$Q_{\text{rot}} = \frac{8\pi^2}{\sigma_{\text{rot}}} \left(\frac{1}{2\pi\hbar^2\beta} \right)^{3/2} \sqrt{I_1^{\text{rot}} I_2^{\text{rot}} I_3^{\text{rot}}} \quad (11)$$

where σ_{rot} is the symmetry number of rotation [43], which is automatically calculated by the program by recognizing the point group symmetry of the species, and I_i^{rot} ($i = 1, 2$ or 3) is the

i -th principal moment of inertia. In the case of a linear molecule the rotational partition function is:

$$Q_{\text{rot}} = \frac{1}{\sigma_{\text{rot}}} \frac{2I}{\hbar^2 \beta} \quad (12)$$

where I is the moment of inertia. *Pilgrim* calculates the rotational partition function of a nonlinear molecule by Eq. (11) and for a linear molecule by Eq. (12), so it includes the permutational symmetry of the wave function due to quantum statistics in an average way. A more subtle issue concerning the fermionic nature of the protons is the antisymmetrization of nuclear motion wave functions. The deviation of the an accurate treatment of the fermionic character of the proton motion from that afforded by the use of symmetry numbers is a very small effect (1 % or less) at most practical temperatures, although the effect may be larger for the ortho-para H + H₂ reaction at low temperature [44–46].

The vibrational partition function in the HO approximation is given by the product of its individual normal mode partition functions

$$Q^{\text{HO}} = \prod_{m=1}^F \frac{e^{-\beta \hbar \omega_m / 2}}{1 - e^{-\beta \hbar \omega_m}} \quad (13)$$

where F is the number of vibrational modes ($3N - 6$ for a non-linear molecule and $3N - 5$ for a linear molecule, N being the number of atoms); ω_m is the HO frequency of the m -th normal mode. Sometimes, it is convenient to separate the HO zero-point energy (ZPE, \mathcal{E}^{HO}),

$$\mathcal{E}^{\text{HO}} = \sum_{m=1}^F \frac{1}{2} \hbar \omega_m \quad (14)$$

so Eq. (13) can be rewritten as

$$Q^{\text{HO}} = \tilde{Q}^{\text{HO}} e^{-\beta \mathcal{E}^{\text{HO}}} \quad (15)$$

where \tilde{Q}^{HO} is the HO vibrational partition function calculated by taking the ZPE as the reference energy

$$\tilde{Q}^{\text{HO}} = \prod_{m=1}^F \frac{1}{1 - e^{-\beta \hbar \omega_m}} \quad (16)$$

The QH approximation includes a multiplicative scale factor λ^{ZPE} that was previously parametrized (for a given level of electronic structure theory) by using a set of experimental ZPE [47, 48]. Specifically,

$$\mathcal{E}^{\text{QH}} = \lambda^{\text{ZPE}} \mathcal{E}^{\text{HO}} \quad (17)$$

and

$$Q^{\text{QH}} = \tilde{Q}^{\text{QH}} e^{-\beta \mathcal{E}^{\text{QH}}} \quad (18)$$

where

$$\tilde{Q}^{\text{QH}} = \prod_{m=1}^F \frac{1}{1 - e^{-\beta \hbar \lambda^{\text{ZPE}} \omega_m}} \quad (19)$$

Notice that in the literature there are scale factors for harmonic frequencies λ^{H} , for fundamentals λ^{F} , and for zero-point energies λ^{ZPE} . The accuracy of the ZPE is most important for partition functions at low and moderate temperatures and for the tunneling effect (Section 2.7).

Therefore λ^{ZPE} is the recommended parameter to use in order to reproduce the correct ZPE. The keyword to introduce the value of λ^{ZPE} in *Pilgrim* is called `freqscale`, and it can be specified for each species inside `pif.struct`. In such a way, minima and transition states may have different values of λ^{ZPE} . This may be convenient because the standard scale factors are parametrized using equilibrium structures, and one may want to use them only for reactants (with a transition-state-specific nonstandard value for transition states). Actually, for some systems, the calculation of λ^{ZPE} for transition states using degeneracy corrected second-order perturbation theory leads to substantially different values from that for minima, and this may have an important effect on the kinetics of the process [49, 50].

The partition functions of all species are calculated with the command

```
pilgrim.py --pfn
```

and an output file is created for each `ctcname` species defined in `pif.struct`. For example, Listing A.5 shows the output file for species H2.

For species with multiple conformations, *Pilgrim* calculates multi-structural harmonic oscillator (MS-HO) or multi-structural quasi-harmonic (MS-QH) partition functions. For simplicity, hereafter, we refer to HO or MS-HO partition functions, although the same arguments are valid for QH and MS-QH partition functions by specifying a value of λ^{ZPE} different than the unity. The MS-HO partition function for a system with N_c distinguishable conformational minima is given by

$$Q^{\text{MS-HO}} = \sum_{n_c=0}^{N_c-1} Q_{n_c}^{\text{RRHO}} e^{-\beta U_{n_c}} \quad (20)$$

where U_{n_c} is the energy of conformer n_c relative to the global minimum. *Pilgrim* evaluates a similar equation to Eq. (20) but incorporating the weight of each conformation as specified in Section 2.2:

$$Q^{\text{MS-HO}} = \sum_{n=0}^{N-1} w_n Q_n^{\text{RRHO}} e^{-\beta U_n} \quad (21)$$

where N runs over all conformations to which we have discounted the enantiomers. The contribution, χ_n , of the n -th structure to the total MS-HO partition function is also calculated:

$$\chi_n = w_n e^{-\beta U_n} \frac{Q_n^{\text{RRHO}}}{Q^{\text{MS-HO}}} \quad (22)$$

The results of applying Eq. (21) to ethanol are shown in Listing A.6.

Pilgrim can also include torsional anharmonic corrections to the partition functions by reading the output files of either the Q2DTor [35] or the MSTor [36, 37] program. Q2DTor can be used to calculate anharmonic hindered rotor partition functions for systems with two coupled torsions by the extended two-dimensional torsional (E2DT) method [51, 52]. The corresponding E2DT anharmonic coefficient, which is temperature dependent, is given by

$$\lambda^{\text{E2DT}}(T) = \frac{Q^{\text{E2DT}}(T)}{Q^{\text{MS-HO}}(T)} \quad (23)$$

Similarly, MSTor can be used to include torsional anharmonicity in molecular systems having many torsions. The multi-structural torsional (MS-T) method implemented in MSTor only

requires, as input, information about the equilibrium structures [53]. The MS-T anharmonic coefficient is given by

$$\lambda^{\text{MS-T}}(T) = \frac{Q^{\text{MS-T}}(T)}{Q^{\text{MS-HO}}(T)} \quad (24)$$

Both E2DT and MS-T treat torsions in a more sophisticated and accurate way than is afforded by 1D treatments because they incorporate couplings in the kinetic and potential energies. *Pilgrim* can use the anharmonic partition functions provided by these programs by specifying the `anhar` keyword in the `pif.struc` file and the location of the output files of the `Q2DTor` or `MSTor` programs.

2.4. Output for conventional TST calculations

The calculation of TST or MS-TST thermal rate constants can be carried out right after the calculation of the partition functions. Notice that the former is a special case of the latter in which the reactants and the transition state do not have torsional conformers. The TST or MS-TST thermal rate constant is given by

$$k^{\ddagger} = \frac{1}{h\beta} \frac{Q^{\ddagger}}{Q_{\text{R}}} e^{-\beta U_0^{\ddagger}} \quad (25)$$

where Q^{\ddagger} and Q_{R} are the total partition functions [Eq. (7)] of the transition state and of reactants, respectively, and U_0^{\ddagger} is the energy difference between the transition state and the reactants. Equation (25) can be rewritten as

$$k^{\ddagger} = B \frac{Q_{\text{rv}}^{\ddagger}}{Q_{\text{rv,R}}} e^{-\beta U_0^{\ddagger}} \quad (26)$$

where Q_{rv}^{\ddagger} and $Q_{\text{rv,R}}$ are the rovibrational partition functions of the transition state and reactants, and

$$B = \frac{1}{h\beta} \frac{Q_{\text{el}}^{\ddagger}}{Q_{\text{el,R}}} \frac{1}{\Phi_{\text{rel}}} \quad (27)$$

is a coefficient that includes the electronic partition functions (Q_{el}) of the transition state (\ddagger) and of the reactants (R) and the relative translational motion of the reactants per unit volume, Φ_{rel} , given by

$$\Phi_{\text{rel}} = \left(\frac{\mu}{2\pi\beta\hbar^2} \right)^{3/2} \quad (28)$$

where μ is the reduced mass of reactants. For unimolecular reactions, Φ_{rel} is replaced by unity. For the case of multiple conformations the rovibrational partition functions are multi-structural, and U_0^{\ddagger} in Eq. (26) is the difference in electronic energy between the transition state structure with the lowest energy and the most stable reactant.

In the thermodynamic formulation Eq. (25) is given by

$$k^{\ddagger} = \frac{1}{h\beta c^{\circ}} \exp\left(-\Delta G^{\ddagger,\circ}/RT\right) \quad (29)$$

where c° is the standard state concentration taken to be 1 molecule/cm³ for bimolecular reactions and the unity (dimensionless) for unimolecular reactions; R is the gas constant; and $\Delta G^{\ddagger,\circ}$ is the standard state free energy of activation between the reactants and the transition state. Notice that *Pilgrim* also lists free energies using $p^{\circ} = 1$ bar standard state.

The thermal rate constants for the reactions specified in the *pif.chem* file can be calculated by typing

```
pilgrim.py --rcons
```

In the case of reaction **R1h**, both the reactants and the transition state have conformers and, therefore, the program calculates the MS-TST thermal rate constant. The output file is displayed in Listing A.7. If products are also specified, *Pilgrim* calculates the equilibrium constant as

$$K_{\text{eq}} = \frac{Q_{\text{P}}}{Q_{\text{R}}} e^{-\beta U_{\text{r}}} \quad (30)$$

where Q_{R} and Q_{P} are the total partition functions of reactants and products, respectively; U_{r} is the difference in potential energy between the most stable product and the most stable reactant. The backward reaction rate constant is calculated from the forward rate constant and the equilibrium constant.

The calculation of recrossing transmission coefficient requires the specification of a reaction path. In *Pilgrim* this path is the minimum energy path (MEP) [24, 54–56]. The following sections describe the algorithms implemented to calculate the MEP and how this information is used to evaluate the variational effects and the quantum effects by the small-curvature tunneling approximation.

2.5. The minimum energy path

The MEP can be defined as the steepest-descent path in isoinertial coordinates that goes from the transition state toward reactants and toward products. The progression along the MEP, s (zero at the transition state), is less than zero in the reactant region and greater than zero in the product region. An infinitesimal progression along this path is given by:

$$ds = \left[\sum_{i=1}^N \sum_{\alpha=x,y,z} dx_{i\alpha}^2 \right]^{1/2} \quad (31)$$

where N is the number of atoms, $x_{i\alpha}$ are mass-scaled coordinates [$\alpha = (x, y, \text{ or } z)$], which are related to the Cartesian coordinates $R_{i\alpha}$ by:

$$x_{i\alpha} = \left(\frac{m_i}{\mu} \right)^{1/2} R_{i\alpha} \quad (32)$$

with μ being the scaling mass. The most common value for this mass is 1 amu,⁷ although for bimolecular reactions it is also common to use the reduced mass of reactants. The differential equation that defines the MEP is

$$\frac{d\mathbf{x}}{ds} = -\hat{\mathbf{G}}(\mathbf{x}) = \mathbf{v}(\mathbf{x}) \quad (33)$$

where \mathbf{x} is the mass-scaled Cartesian coordinates vector, $\hat{\mathbf{G}}$ is the normalized gradient and \mathbf{v} is the vector with opposite direction to the gradient.

⁷Default value in *Pilgrim* ; keyword mu.

Due to the fact that the gradient at the transition state structure is zero, the first geometry along the MEP, $\mathbf{x}(s_1)$, can be defined in the direction of the eigenvector of the mode with imaginary frequency, $\mathbf{L}_F(\mathbf{x}^\ddagger)$, using a step size of δs :

$$\mathbf{x}(s_1 = \pm\delta s) = \mathbf{x}^\ddagger \pm \delta s \mathbf{L}_F(\mathbf{x}^\ddagger) \quad (34)$$

The $\mathbf{L}_F(\mathbf{x}^\ddagger)$ eigenvector is obtained by diagonalization of the Hessian matrix in iso-inertial coordinates $\mathbf{F}(\mathbf{x}^\ddagger)$ at the transition state:

$$\mathbf{L}(\mathbf{x}^\ddagger)^\dagger \mathbf{F}(\mathbf{x}^\ddagger) \mathbf{L}(\mathbf{x}^\ddagger) = \mathbf{\Lambda}(\mathbf{x}^\ddagger) \quad (35)$$

where \mathbf{x}^\ddagger is the geometry at the transition state; \dagger denotes a transpose; and $\mathbf{L}(\mathbf{x}^\ddagger)$ is a orthonormal square matrix composed $3N$ columns that are the normal mode eigenvectors. There are F eigenvectors corresponding to vibrations where F is $3N - 6$ for a nonlinear molecule and $3N - 5$ for a linear molecule, with N being the number of atoms. The $3N \times 3N$ diagonal matrix, $\mathbf{\Lambda}(\mathbf{x}^\ddagger)$, contains the $3N$ eigenvalues $\lambda_m(\mathbf{x}^\ddagger)$, of which $3N - F$ should be zero (translations and rotations) and the remaining F eigenvalues are related to the normal mode frequencies of the transition state $\omega_m(s=0)$ by

$$\omega_m(s=0) = [\lambda_m(\mathbf{x}^\ddagger) / \mu]^{1/2} \quad (36)$$

Because we are discussing a first-order saddle point, $F - 1$ eigenvalues are real and $\lambda_F(\mathbf{x}^\ddagger)$ is imaginary.

A more accurate method to obtain the first point along the MEP, although more expensive, was proposed by Page and McIver in which the potential energy surface around the saddle point is expanded to cubic or higher order terms. For the case of cubic expansion, the curvature vector at the saddle point $\mathbf{c}(\mathbf{x}^\ddagger)$ is given by

$$\mathbf{c}(\mathbf{x}^\ddagger) = [2\mathbf{L}_F^\dagger \mathbf{F}(\mathbf{x}^\ddagger) \mathbf{L}_F(\mathbf{x}^\ddagger) \mathbf{I} - \mathbf{F}(\mathbf{x}^\ddagger)]^{-1} [\mathbf{C}(\mathbf{x}^\ddagger) \mathbf{L}_F(\mathbf{x}^\ddagger) - \mathbf{L}_F^\dagger(\mathbf{x}^\ddagger) \mathbf{C}(\mathbf{x}^\ddagger) \mathbf{L}_F(\mathbf{x}^\ddagger) \mathbf{L}_F(\mathbf{x}^\ddagger)] \quad (37)$$

and the first point along the reaction path is given by:

$$\mathbf{x}(s_1 = \pm\delta s) = \mathbf{x}^\ddagger \pm \delta s \mathbf{L}_F(\mathbf{x}^\ddagger) \pm \frac{1}{2}(\delta s)^2 \mathbf{c}(\mathbf{x}^\ddagger) \quad (38)$$

where the calculation of $\mathbf{C}(\mathbf{x}^\ddagger)$ involves the computation of two additional Hessian matrices, one on each side of the saddle point and away from it by δ_3 in the direction of $\mathbf{L}_F(\mathbf{x}^\ddagger)$

$$\mathbf{C}(\mathbf{x}^\ddagger) = \frac{d\mathbf{F}}{ds} \approx \frac{\mathbf{F}(\mathbf{x}^\ddagger + \delta_3 \mathbf{L}_F(\mathbf{x}^\ddagger)) - \mathbf{F}(\mathbf{x}^\ddagger - \delta_3 \mathbf{L}_F(\mathbf{x}^\ddagger))}{2\delta_3} \quad (39)$$

The first step using Eq. 38 can be turned on by adding the `cubic` keyword in the `pif.path` file.

After the first point along the MEP, the remaining steps can be calculated by a first-order approximation (the Euler algorithm [56]) where the $(n+1)$ -th geometry along the MEP, \mathbf{x}_{n+1} , is calculated from the gradient \mathbf{G}_n and the geometry of the previous step, \mathbf{x}_n :

$$\mathbf{x}_{n+1} = \mathbf{x}_n - \delta s \hat{\mathbf{G}}_n = \mathbf{x}_n + \delta s \mathbf{v}_n \quad (40)$$

A higher-order method to follow the MEP, which corrects the path by means of Hessian calculations, was proposed by Page and McIver [57, 58] (see B).

The information stored along the MEP can be used to calculate the reaction-path curvature coupling elements $B_{m,F}$ between the reaction coordinate and a mode m perpendicular to it [55]. They are obtained at every point along the MEP at which a Hessian is calculated and are given by:

$$B_{m,F} = -[\text{sign}(s)] \frac{d\hat{\mathbf{v}}(s)}{ds} \mathbf{L}_m(s) = -[\text{sign}(s)] \sum_{i=0}^{3N} \frac{d\hat{v}_i(s)}{ds} L_{i,m}(s) \quad (41)$$

where, as already noted, $\hat{\mathbf{v}}(s) = -\hat{\mathbf{G}}(s)$ and the eigenvectors $\mathbf{L}_m(s)$ are obtained from the diagonalization of the Hessian matrix at s . The derivative of $\mathbf{v}(s)$ is obtained by finite differences

$$\frac{d\hat{v}_i(s)}{ds} = \frac{\hat{v}_i[s + \delta s \text{sign}(s)] - \hat{v}_i[s - \delta s \text{sign}(s)]}{2\delta s} \quad (42)$$

A different way of evaluating the coupling elements was given by Page and McIver in which the derivatives of the gradient are not needed:

$$B_{m,F} = -[\text{sign}(s)] \mathbf{L}_m^\dagger(s) \mathbf{F}(s) \hat{\mathbf{v}}(s) \quad (43)$$

We highlight that performing Hessian calculations at every point along the MEP can be very expensive. A common practice is to employ the same Hessian for N_H steps before recalculating it. A recommended value for N_H is 9 [56]. Consequently, the resulting distance between Hessian evaluations is:

$$\delta s_H = N_H \delta s \quad (44)$$

Currently, both the Euler [56] and the Page-McIver [57] algorithms are implemented in *Pilgrim* to follow the MEP. We highlight that the calculation of VTST coefficients requires Hessian calculations along the MEP. Interestingly, the Page-McIver algorithm makes use of the Hessian matrices for a better estimation of the MEP points, whereas the Euler algorithm ignores them. Consequently, both algorithms will require equivalent computational cost but the Page-McIver MEP will be undoubtedly closer to the real MEP. For this reason, *Pilgrim* uses the Page-McIver algorithm by default.

2.6. Input files for calculating the MEP

The basic input for the MEP calculation can be generated by typing:

```
> add path ctcts
```

which for the case of **R1h** is

```
> add path TSoh
```

After execution of this command, the program creates two files: (1) *pif.path*, which contains some of the parameters associated with the MEP; and (2) *pif.calcs*, which contains the template for the ESSO. A complete list of the keywords that can be used in the *pif.path* file is given in *Pilgrim*'s manual.

Pilgrim has two criteria to decide whether the MEP has reached a minimum. The first one is an energy criterion in which the MEP calculation stops if the difference in energy between two

consecutive points along the MEP is smaller than $10^{-8}E_h$, E_h being a hartree. The second one stops the MEP calculation if the magnitude of the gradient, $|\mathbf{G}|$, is smaller than $10^{-8}E_h/a_0$. The two thresholds can be modified using the `eps` and `epsG` keywords.

The electronic structure calculations required along the MEP are carried out using a ESSO. Listing A.8 shows the default template for *Gaussian* package as the ESSO. This template can be modified in the same way as a standard *Gaussian* input file, the only exception being the keywords between square brackets, which are for *Pilgrim*'s internal use and should not be modified.

2.7. Variational and tunneling effects

For reactions with several conformational structures of the transition state, full multipath VTST calculations involve the evaluation of the MEP for each of the distinguishable conformations excluding conformational enantiomers. With that information at hand, *Pilgrim* calculates variational effects by using canonical variational transition state theory (CVT) and calculates quantum effects in the reaction coordinate by using the small-curvature tunneling approximation. Equation (2) for each transition state structure j becomes

$$\gamma_j^{\text{CVT/SCT}} = \Gamma_j^{\text{CVT}} \kappa_j^{\text{CVT/SCT}} \quad (45)$$

A rate constant as a function of the position of the transition state along the reaction path is called a generalized transition state (GT) rate constant and it is given by

$$k_j^{\text{GT}}(T, s) = B(T) \frac{Q_{\text{rv},j}^{\text{GT}}(T, s)}{Q_{\text{rv},\text{R}}(T)} e^{-\beta U_{\text{MEP},j}(s)} \quad (46)$$

The value of Γ_j^{CVT} at a given temperature is calculated by finding the minimum of $k_j^{\text{GT}}(T, s)$ as a function of s :

$$k_j^{\text{CVT}}(T) = \min_s [k_j^{\text{GT}}(T, s)] \quad (47)$$

which is equivalent to finding the maximum of the generalized free energy of activation along the reaction path. With s_{\star}^{CVT} being the value of s that minimizes the GT rate constant at a given temperature, we can write:

$$k_j^{\text{CVT}}(T) = B(T) \frac{Q_{\text{rv},j}^{\text{GT}}(T, s_{\star}^{\text{CVT}})}{Q_{\text{rv},\text{R}}(T)} e^{-\beta U_{\text{MEP},j}(s_{\star}^{\text{CVT}})} \quad (48)$$

where $Q_{\text{rv},j}^{\text{GT}}(T, s_{\star}^{\text{CVT}})$ is the GT rovibrational partition function at s_{\star}^{CVT} assuming the same rotational symmetry number in the calculation of the rotational partition function as the transition state. Equation (48) can also be written as:

$$k_j^{\text{CVT}}(T) = \frac{1}{h\beta c^{\circ}} \exp(-\Delta G_j^{\text{CVT},\circ}(T)/RT) \quad (49)$$

where $\Delta G_j^{\text{CVT},\circ}$ is the standard-state free energy of activation at $s = s_{\star}^{\text{CVT}}$, which is the location where the generalized standard-state free energy of activation along the MEP has a maximum [27].

Taking into account that the variational effects for each of the transition states are obtained from Eq (3), then

$$\Gamma_j^{\text{CVT}}(T) = \frac{k_j^{\text{CVT}}(T)}{k_j^{\ddagger}(T)} \quad (50)$$

Because $k_j^{\text{CVT}}(T)$ is given by Eq. (48) and $k_j^\ddagger(T)$ by the same equation but at the saddle point ($s = 0$), we have that

$$\Gamma_j^{\text{CVT}}(T) = \frac{Q_{\text{rv},j}^{\text{GT}}(T, s_\star^{\text{CVT}})}{Q_{\text{rv},j}^\ddagger(T)} e^{-[\beta \Delta U_j(s_\star^{\text{CVT}})]} \quad (51)$$

where

$$\Delta U_j(s_\star^{\text{CVT}}) = U_{\text{MEP},j}(s_\star^{\text{CVT}}) - U_{0,j} \quad (52)$$

Equation (51) is independent of the reactants and it only depends on the properties of the transition state. The difference in generalized free energy of activation between the variational transition state and the conventional transition state at $s = 0$ is

$$\Delta \Delta G_{\text{var},j}^0(T) = \Delta G_j^{\text{CVT},0}(T) - \Delta G_j^{\ddagger,0}(T) = -RT \log [\Gamma_j^{\text{CVT}}(T)] \quad (53)$$

In the MP version of the theory, multidimensional tunneling effects are incorporated for each transition structure and associated reaction path, through a multiplicative tunneling transmission coefficient that includes the coupling between the reaction coordinate and the $F - 1$ degrees of freedom perpendicular to it. This coefficient is given by the ratio between the Boltzmann averaged semiclassical adiabatic ground-state probability, P^{SAG} , and the classical one.⁸ The resulting expression after integration of the classical probability is

$$\kappa^{\text{SAG}} = \frac{\beta \int_0^\infty dE \exp(-\beta E) P^{\text{SAG}}(E)}{\exp(-\beta V^{\text{AG}})} \quad (54)$$

where

$$P^{\text{SAG}}(E) = \begin{cases} 0, & E < E_0 \\ \{1 + \exp[2\theta(E)]\}^{-1}, & E_0 \leq E \leq V^{\text{AG}} \\ 1 - P^{\text{SAG}}(2V^{\text{AG}} - E), & V^{\text{AG}} \leq E \leq 2V^{\text{AG}} - E_0 \\ 1, & 2V^{\text{AG}} - E_0 < E \end{cases} \quad (55)$$

For each tunneling energy on a grid of energies, *Pilgrim* calculates two SAG action integrals, $\theta(E)$, and therefore two SAG tunneling probabilities: the zero-curvature tunneling (ZCT) [59] and the small-curvature tunneling (SCT) [28–30] probabilities (see C for details). The semiclassical probability of Eq. (55) includes tunneling effects (usually the main contribution to the transmission coefficient) for energies below the maximum, V^{AG} , of the vibrationally adiabatic ground-state potential and nonclassical reflection using a parabolic extension for energies above that maximum. In the harmonic approximation, the vibrationally adiabatic ground-state potential is calculated along the MEP as

$$V_a^{\text{G}}(s) = V_{\text{MEP}}(s) + \sum_m^{F-1} \frac{\hbar \omega_m(s)}{2} \quad (56)$$

where $\omega_m(s)$ are the projected frequencies at a given value of s .

The transmission coefficient given by Eq. (54) and based on the transmission probability of Eq. (55) is calculated for an effective potential with a maximum located at the highest value of the

⁸Note that in the present context, “ground-state” refers to the ground vibrational state of the transverse vibrational modes along a given reaction path.

vibrationally adiabatic potential, V^{AG} . If one treats the transmission probability classically with this effective potential, the classical step function would rise at V^{AG} , but this threshold may not coincide with that implied by TST or CVT thermal rate constants for the case where tunneling is neglected. The former has its threshold at $V_a^{\ddagger\text{G}} = V_a^{\text{G}}(s=0)$, and the latter has its threshold at $V_a^{\text{G}}[s_{\star}^{\text{CVT}}(T)]$. To make the transmission coefficient consistent with the theories to which they are being added, the transmission coefficient for conventional TST should be multiplied by

$$\kappa^{\text{TST/CAG}} = \exp\left[\beta\left(V_a^{\ddagger\text{G}} - V^{\text{AG}}\right)\right] \quad (57)$$

and that for CVT should be multiplied by

$$\kappa^{\text{CVT/CAG}} = \exp\left\{\beta\left[V_a^{\text{G}}\left(s_{\star}^{\text{CVT}}(T)\right) - V^{\text{AG}}\right]\right\} \quad (58)$$

These are called classical adiabatic ground-state (CAG) coefficients. Due to these factors the tunneling transmission coefficient that multiplies the conventional TST thermal rate constant is:

$$\kappa^{\text{TST/SAG}} = \kappa^{\text{TST/CAG}} \kappa^{\text{SAG}} \quad (59)$$

and the one that multiplies the CVT thermal rate constant is

$$\kappa^{\text{CVT/SAG}} = \kappa^{\text{CVT/CAG}} \kappa^{\text{SAG}} \quad (60)$$

Notice that $\kappa^{\text{TST/SAG}}$ and $\kappa^{\text{CVT/SAG}}$ may be smaller than the unity due to the threshold correction since $\kappa^{\text{TST/CAG}}$ and $\kappa^{\text{CVT/CAG}}$ are always smaller or equal to the unity. However, $\kappa^{\text{SAG}} \geq 1$, and it can be shown that

$$\kappa^{\text{SAG}} = 1 + 2\beta \int_{E_0}^{V^{\text{AG}}} P^{\text{SAG}}(E) \sinh\left[\beta\left(V^{\text{AG}} - E\right)\right] \quad (61)$$

Although *Pilgrim* calculates SAG probabilities for both ZCT and SCT, rest of the discussion will refer mainly to the SCT approximation, because is more accurate than the ZCT approximation.

2.8. Quantized-reactant-states tunneling calculations

For unimolecular reactions at low temperatures, the continuum of energy states in the integration of Eq. (54) is better represented by a discrete sum over energy levels for energies below V^{AG} [60, 61]. In this situation the semiclassical adiabatic ground-state transmission coefficient is given by

$$\kappa^{\text{SCT}} = \frac{\beta \sum_{v=0}^K \frac{dE_v^{\text{R}}}{dv} P^{\text{SCT}}(E_v^{\text{R}}) \exp(-\beta E_v^{\text{R}}) + \beta \int_{V^{\text{AG}}}^{\infty} dE \exp(-\beta E) P^{\text{SCT}}(E)}{\exp(-\beta V^{\text{AG}})} \quad (62)$$

where K is the maximum value that the quantum number v can reach when exciting the discrete levels of the reaction coordinate motion E_v^{R} up to V^{AG} . The reaction coordinate levels are

$$E_v^{\text{R}} = \left(\frac{1}{2} + v\right) \hbar\omega_F^{\text{R}} \quad (63)$$

where ω_F^{R} is the reaction coordinate frequency. Notice that

$$\frac{dE_v^{\text{R}}}{dv} = \hbar\omega_F^{\text{R}} \quad (64)$$

Pilgrim offers the possibility of using Eq. (62) for unimolecular reactions.

2.9. Redundant internal coordinates

At stationary points, normal-mode vibrational frequencies do not depend on the choice of coordinates, but when calculated at non-stationary points, the frequencies are coordinate dependent [62]. Because the generalized free energies of activation and vibrationally adiabatic potentials have strong dependences on the vibrational frequencies, it is important to transform the Hessian matrices calculated along the MEP to a physical set of coordinates in order to obtain physical frequencies. It is known that internal coordinates [63], which are curvilinear, provide a more physical description of the vibrations than Cartesian coordinates, [64, 65] which are rectilinear.⁹ Furthermore, using rectilinear coordinates for the vibrational analysis along the reaction path can give physically unreasonable results [62]. When using internal coordinates, one must choose between a nonredundant set, which is sufficient, or a redundant set, which is often more convenient because sometimes it is difficult to find a set of nonredundant internal coordinates that adequately describes the vibrational space.

Calculating the transverse vibrational frequencies along a reaction path requires to project the reaction coordinate out of the Hessian [6]. Methods have been developed for calculating vibrational frequencies along a reaction path in both nonredundant [65–67] and redundant [68] internal coordinates, and *Pilgrim* can evaluate the vibrational frequencies in both cases. The transformation of the Cartesian coordinates, gradient \mathbf{G} , and Hessian \mathbf{F} into internal coordinates is well established [65, 68–74]. See D for details.

Pilgrim provides a set of internal coordinates to each `ctcts`, although it is also possible to generate a different set of coordinates for each transition structure within the `ctcts`. The internal coordinates can be generated by the command

```
pilgrim.py --ics [mode [target[.idx]]]
```

where the values for `mode` are:

- 1: for standard generation of a redundant set
- 2: for the generation of a smaller redundant set (default)
- 3: for the generation of a non-redundant set
- -1: to check a previously generated set
- -2: to delete the current set

and `target` is the label of the species (i.e., a `ctcts`) containing all the transition structures. If `idx` is also specified, the internal coordinates are exclusively generated for that particular transition structure. For instance,

```
pilgrim.py --ics 1 TSoh.001
```

generates a redundant set of internal coordinates for the lowest-energy conformer of `Tsoh`, whereas

⁹Rectilinear coordinates are any coordinates that can be obtained by a linear transformation from atomic Cartesians, whereas curvilinear coordinates are related nonlinearly to atomic Cartesians.

```
pilgrim.py --ics 1 TSoh
```

generates a redundant set of internal coordinates common to all the conformers (i.e., all the structures) of TSoh. The resulting internal coordinates are included in the *pif.struc* file as shown in Listing A.9.

2.10. Output of MEP calculations

The information provided in the *pif.struc*, *pif.path* and *pif.calcs* input files allows *Pilgrim* to calculate the MEP after the command

```
pilgrim.py --path
```

is executed. *Pilgrim* calculates the MEP by successive calls to the ESSO until the values of *sbw* and *sfw* for each *ctcts* are reached or until the MEP convergence criteria are fulfilled. In the example here presented, both *ctcts* (TSoh and TSod) are run between $-2.00 \cdot a_o$ and $2.00 \cdot a_o$ with a stepsize of $0.01 \cdot a_o$ and Hessian calculations every $N_H = 10$ steps.¹⁰ Once the MEP is obtained, *Pilgrim* prints a table with the energy of each point (see Listing A.10 for the case of TSoh.001).

The vibrationally adiabatic ground-state potential is calculated from the Cartesian-coordinate Hessian, although this is not the recommended procedure. If internal coordinates are available, the program also produces the vibrationally adiabatic potential based on them, and it is recommended to use this for the rate constant calculations. If both vibrationally adiabatic potentials are available, the program always uses the one obtained with internal coordinates (see Listing A.11).

The variational coefficients and the TST/CAG and CVT/CAG transmission coefficients are obtained from Eqs. (53), (57) and (58), respectively (Listing A.12).

Tunneling effects are included by plugging the ZCT and SCT tunneling probabilities into Eq. (54). Listing A.13 includes information listed by *Pilgrim* after performing a tunneling calculation. *Pilgrim* also lists the contribution in percentage to the transmission coefficient of two energy intervals

$$\kappa^{SAG} = \frac{\int_0^{V^{AG}} dE e^{-\beta E} P^{SAG}(E) + \int_{V^{AG}}^{\infty} dE e^{-\beta E} P^{SAG}(E)}{\beta^{-1} \exp(-\beta V^{AG})} \quad (65)$$

where the first integral represents the contribution due to tunneling and the second integral is the contribution due to nonclassical reflection. In Listing A.13 the contribution due to tunneling in the case of the SCT approximation at $T = 298.15$ K is 97.75%, and the κ^{SCT} transmission coefficient is 27.68. *Pilgrim* also lists the representative tunneling energy (RTE), that is, the energy at which the product of the tunneling probability and the Boltzmann factor is a maximum. This product is the integrand in the above integral, and so its maximum gives the energy at which the greatest number of particles tunnel. Finally, the program prints a summary with the Γ^{CVT} , κ^{ZCT} , κ^{SCT} , $\kappa^{TST/CAG}$ and $\kappa^{CVT/CAG}$ coefficients. Notice that the final CVT/SCT coefficient is given by Eq. (45).

Although we have dropped the subscript j during the discussion of tunneling, the reader should note that in multipath calculations the variational, tunneling, and CAG coefficients have to be calculated for each transition structure.

¹⁰All distances are in the mass-weighted coordinates of Eq. 32

2.11. Multi-structural and multipath CVT/SCT rate constants

The multi-structural CVT/SCT thermal rate constant (MS-CVT/SCT) is given by the product of the MS-TST rate constant and the CVT/SCT coefficient, $\gamma_0^{\text{CVT/SCT}}$, calculated using the transition structure with the lowest energy (indicated by the subscript 0) within a given CTC. Specifically,

$$k^{\text{MS-CVT/SCT}} = \gamma_0^{\text{CVT/SCT}} k^\ddagger \quad (66)$$

where k^\ddagger is the MS-TST thermal rate constant and

$$\gamma_0^{\text{CVT/SCT}} = \Gamma_0^{\text{CVT}} k_0^{\text{CVT/SCT}} \quad (67)$$

The MP-CVT/SCT thermal rate constant, $k^{\text{MP-CVT/SCT}}$, is calculated as the sum of the individual CVT/SCT rate constants, defined as the product between the CVT/SCT coefficient and the individual conventional TST thermal rate constant, k_j^\ddagger , calculated for each of the transition structures:

$$k^{\text{MP-CVT/SCT}}(T) = \sum_{j=0}^{J^\ddagger-1} \gamma_j^{\text{CVT/SCT}}(T) k_j^\ddagger(T) \quad (68)$$

$$k_j^\ddagger(T) = B(T) \frac{Q_{\text{rv},j}^\ddagger(T)}{Q_{\text{rv,R}}^{\text{MS-HO}}(T)} e^{-\beta U_0^\ddagger} \quad (69)$$

An average CVT/SCT coefficient $\langle \gamma^{\text{CVT/SCT}}(T) \rangle$ for the multipath thermal rate constant can be calculated as the ratio

$$\langle \gamma^{\text{CVT/SCT}}(T) \rangle = \frac{k^{\text{MP-CVT/SCT}}(T)}{k^\ddagger(T)} \quad (70)$$

where $k^\ddagger(T)$ is the MS-TST rate constant. Notice that $\langle \gamma^{\text{CVT/SCT}}(T) \rangle$ does not depend on the properties of reactants, and from Eq. (70), we obtain that

$$\langle \gamma^{\text{CVT/SCT}}(T) \rangle = \frac{\sum_j \gamma_j^{\text{CVT/SCT}}(T) w_j^\ddagger Q_j^{\text{RRHO},\ddagger}(T) e^{-\beta U_j^\ddagger}}{Q_{\text{rv}}^{\text{MS-HO},\ddagger}(T)} \quad (71)$$

where

$$Q_{\text{rv}}^{\text{MS-HO},\ddagger}(T) = \sum_j w_j^\ddagger Q_j^{\text{RRHO},\ddagger}(T) e^{-\beta U_j^\ddagger} \quad (72)$$

which is analogous to Eq. (21).

Pilgrim also calculates the contribution of each transition state conformer (i.e., each transition structure) to the MP-CVT/SCT rate constant, given by:

$$\chi_j^{\text{MP-CVT/SCT}} = \frac{\gamma_j^{\text{CVT/SCT}} k_j^\ddagger}{k^{\text{MP-CVT/SCT}}} \quad (73)$$

or, generalized for any method X:

$$\chi_j^{\text{MP-X}} = \frac{\gamma_j^{\text{X}} k_j^\ddagger}{k^{\text{MP-X}}} \quad (74)$$

Using Eq. (70) each contribution can be expressed as:

$$\chi_j^{\text{MP-X}} = \frac{\gamma_j^{\text{X}} k_j^\ddagger}{\langle \gamma^{\text{X}} \rangle k^\ddagger} = \frac{\gamma_j^{\text{X}}}{\langle \gamma^{\text{X}} \rangle} \chi_j^{\text{MS-TST}} \quad (75)$$

where $\chi_j^{\text{MS-TST}}$ is the contribution of the j -th transition state conformer to the MS-TST rate constant, which matches with its contribution to the MS-HO partition function shown in Eq. (22).

As in the case of MS-TST, the VTST rate constants are calculated by typing

```
pilgrim.py --rcons
```

Pilgrim lists the $\langle \gamma^{\text{CVT/SCT}}(T) \rangle$ coefficient as shown in Listing A.14. *Pilgrim* also lists the contribution of each of the transition structures to the MP-TST/ZCT, MP-TST/SCT, MP-CVT, MP-CVT/ZCT and MP-CVT/SCT thermal rate constants. The thermal rate constants corresponding to the passage from reactants to products (forward) are shown in Listing A.15. If products have been defined in the *pif.chem* file, the backward thermal rate constants are also calculated using microscopic reversibility.

2.12. Kinetic isotope effects

Pilgrim can evaluate the contribution of each of the transition structures to the kinetic isotope effect (KIE). For the case of a deuterium KIE, the KIE in the MP-CVT/SCT approximation, $\eta^{\text{MP-CVT/SCT}}$, is given by

$$\eta^{\text{MP-CVT/SCT}} = \frac{k_{\text{H}}^{\text{MP-CVT/SCT}}}{k_{\text{D}}^{\text{MP-CVT/SCT}}} \quad (76)$$

where $k_{\text{H}}^{\text{MP-CVT/SCT}}$ is the thermal rate constant for the protium species, and $k_{\text{D}}^{\text{MP-CVT/SCT}}$ is that for the deuterated species. In the example presented here, it is the ratio between the MP-CVT/SCT thermal rate constants calculated for the **R1h** and **R1d** reactions. Equation (76) can also be written as a weighted sum of individual contributions [75]

$$\eta^{\text{MP-CVT/SCT}} = \sum_{j=0}^{J^{\ddagger}-1} P_{j,\text{D}}^{\text{MP-CVT/SCT}} \eta_j^{\text{CVT/SCT}} \quad (77)$$

where the weight depends exclusively on the properties of the transition structures of the deuterated species

$$P_{j,\text{D}}^{\text{MP-CVT/SCT}} = \frac{w_j^{\ddagger} \gamma_{j,\text{D}}^{\text{CVT/SCT}} Q_{j,\text{D}}^{\text{RRHO},\ddagger}}{\sum_{j=0}^{J^{\ddagger}-1} w_j^{\ddagger} \gamma_{j,\text{D}}^{\text{CVT/MT}} Q_{j,\text{D}}^{\text{RRHO},\ddagger}} \quad (78)$$

and the individual contributions are partitioned into

$$\eta_j^{\text{CVT/SCT}} = \eta_{\text{tor}} \eta_{\text{trans}} \eta_{\text{rv},j}^{\ddagger} \eta_{\text{vtun},j}^{\text{CVT/SCT}} \quad (79)$$

where η_{tor} and η_{trans} are the torsional anharmonic and translational contributions to the KIE. Notice that both contributions are independent of the number of conformations within the CTC and

$$\eta_{\text{tor}} = \frac{\alpha_{\text{H}}}{\alpha_{\text{D}}} \quad (80)$$

where α is the ratio between the torsional anharmonic and torsional harmonic multistructural partition functions (in the numerator for the case of the protium species and in the denominator for the deuterated species). The translational contribution (which is present only for a bimolecular reaction) is the ratio

$$\eta_{\text{trans}} = \frac{\Phi_{\text{rel},\text{D}}}{\Phi_{\text{rel},\text{H}}} \quad (81)$$

The contribution of each of the transition state structures to the rovibrational partition function is

$$\eta_{\text{rv},j}^{\ddagger} = \frac{Q_{\text{R,D}}^{\text{MS-HO}} Q_{j,\text{H}}^{\text{RRHO},\ddagger}}{Q_{\text{R,H}}^{\text{MS-HO}} Q_{j,\text{D}}^{\text{RRHO},\ddagger}} \quad (82)$$

whereas the variational and tunneling contributions are given by

$$\eta_{\text{vtun},j}^{\text{CVT/SCT}} = \frac{\gamma_{j,\text{H}}^{\text{CVT/SCT}}}{\gamma_{j,\text{D}}^{\text{CVT/SCT}}} = \frac{\Gamma_{j,\text{H}}^{\text{CVT}} \kappa_{j,\text{H}}^{\text{CVT/SCT}}}{\Gamma_{j,\text{D}}^{\text{CVT}} \kappa_{j,\text{D}}^{\text{CVT/SCT}}} \quad (83)$$

Equation (77) can be rewritten as:

$$\eta^{\text{MP-CVT/SCT}} = \sum_{j=0}^{J^{\ddagger}-1} \tilde{\eta}_j^{\text{CVT/SCT}} \quad (84)$$

which is a sum of the weighted individual KIEs:

$$\tilde{\eta}_j^{\text{CVT/SCT}} = P_{j,\text{D}}^{\text{MP-CVT/SCT}} \eta_j^{\text{CVT/SCT}} \quad (85)$$

The ratio between the weighted individual KIE and the total KIE provides the contribution of each transition structure to the final KIE:

$$P_{j,\text{H}}^{\text{MP-CVT/SCT}} = \frac{\tilde{\eta}_j^{\text{CVT/SCT}}}{\eta^{\text{CVT/SCT}}} \quad (86)$$

When a transition state has only a single transition structure, the KIE reduces to Eq. (79).

When executed with `--kies`, *Pilgrim* lists the available reactions and asks the user for the unsubstituted and isotopically substituted reactions, as shown in Listing A.16. After the two reactions are selected, the program prints the method-independent contributions (Listing A.17), as well as the total variational-tunneling contribution and the total KIE (Listing A.18) and the different individual contributions obtained by each method (Listing A.19).

3. Study of reaction mechanisms

In this section we discuss the simulation of a reaction mechanism composed of M elementary reactions $\{R_1, \dots, R_i, \dots, R_M\}$ involving a set of K reagents $\{S_1, \dots, S_k, \dots, S_K\}$.¹¹ For each of the reactions R_i the thermal rate constant k_i is assumed to be known. The initial population of the K species is also assumed to be known and is given by

$$\mathbf{x}_0 = \mathbf{x}(t=0) = (x_1(0), \dots, x_k(0), \dots, x_K(0)) \quad (87)$$

The objective is to monitor the time evolution of the populations as a function of time t :

$$\mathbf{x} = \mathbf{x}(t) = (x_1(t), \dots, x_k(t), \dots, x_K(t)) \quad (88)$$

The population vector \mathbf{x} is also called the state vector.

¹¹A reagent is a stable chemical species.

3.1. The kinetic Monte-Carlo algorithm

Pilgrim determines this time evolution by a stochastic method, in particular by kinetic Monte Carlo (KMC) [38, 39]. The fundamental assumption of KMC is that, for each of the elementary reactions, R_i , there is a function, called the propensity function, $a_i(\mathbf{x})$, such that $a_i(\mathbf{x})dt$, represents the probability at time t that reaction R_i will occur inside a given volume V in the infinitesimal time interval $[t, t + dt]$. Here we have indicated that $a_i(\mathbf{x})$ depends on \mathbf{x} , where we use \mathbf{x} to denote the set x_k , where x_k is the number of molecules (or atoms if the species is monatomic) of species S_k . Depending on the type of reaction, the propensity $a_i(\mathbf{x})$ is related to a reaction parameter c_i in such a way that $c_i dt$ provides the probability that a given molecule of species S_k will react in the next infinitesimal time dt . The number of molecules of species S_k that undergo reaction in time dt is $x_k c_i dt$ and therefore $a_i = x_k c_i$. The relation between $a_i(\mathbf{x})$, c_i and k_i for the three possible types of unimolecular and bimolecular reactions is shown in Table 3.

Table 3: Relation between the kinetic equations for elementary reactions, propensities, reaction parameters and rate constants.

Reaction	Kinetic equation	Relation k_i, c_i	Relation c_i, a_i
$S_k \rightarrow P$	$\frac{d[P]}{dt} = k_i[S_k]$	$c_i = k_i$	$\frac{dx_P}{dt} = a_i = c_i x_k$
$S_k + S_{k+1} \rightarrow P$	$\frac{d[P]}{dt} = k_i[S_k][S_{k+1}]$	$c_i = k_i/V$	$\frac{dx_P}{dt} = a_i = c_i x_k x_{k+1}$
$2S_k \rightarrow P$	$\frac{d[P]}{dt} = k_i[S_k]^2$	$c_i \simeq 2k_i/V$	$\frac{dx_P}{dt} = a_i = \frac{1}{2}c_i x_k(x_k - 1)$ $\simeq \frac{1}{2}c_i x_k^2$

The reaction probability density function, $p(\tau, i)$ is derived from the fundamental assumption of KMC and gives the probability at time t that the next reaction in the system will be reaction R_i and that it will occur in the infinitesimal time between $t + \tau$ and $t + \tau + dt$. It is given by

$$p(\tau, i) = a_i \exp[-a_0 \tau] \quad (89)$$

where

$$a_0 = \sum_{i=1}^M a_i \quad (90)$$

The values of τ and i in Eq. (89) are generated by two random numbers r_1 and r_2 , both in the interval between zero and one:

$$\tau = \frac{1}{a_0} \log\left(\frac{1}{r_1}\right) \quad (91)$$

$$\sum_{i'=1}^{i-1} a_{i'} < a_0 r_2 \leq \sum_{i'=1}^i a_{i'} \quad (92)$$

The time τ obtained from Eq. (91) is used to update the time variable, and the value of i is used to identify the reaction that takes place. Because reaction R_i is identified with a one or more reagents, their populations are also updated. The algorithm stops when the population of

the initial reactive species is extinguished or when that population remains stationary due to the reaction system reaching equilibrium. When the algorithm stops, *Pilgrim* prints the total time and the populations of reagents. The KMC algorithm is depicted schematically in Figure 4.

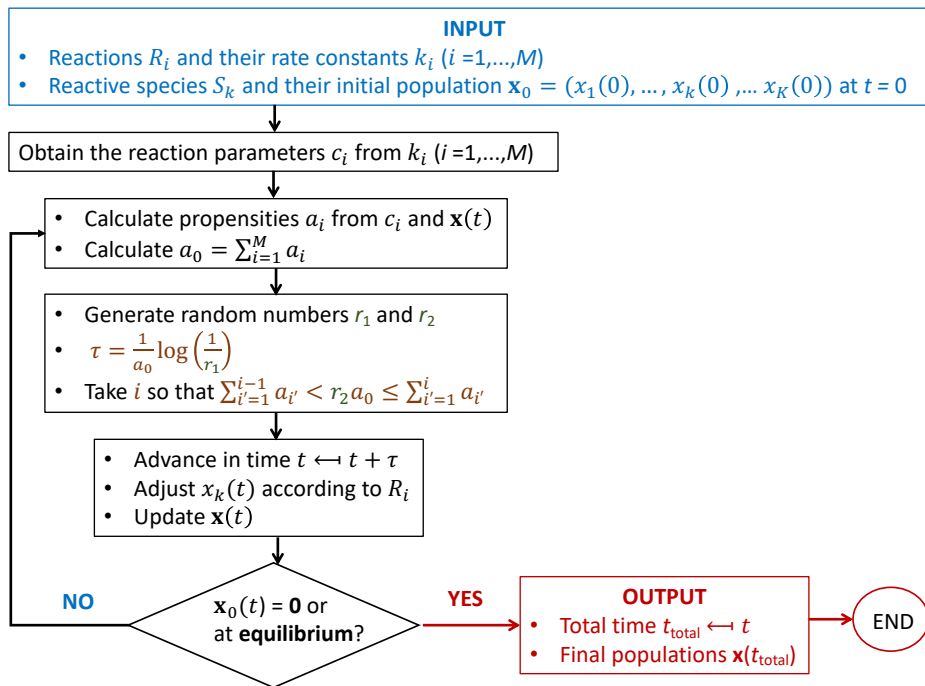


Figure 4: Flow diagram for the KMC algorithm

3.2. Application of KMC

We will consider the chemical reactions involved in a decomposition mechanism of the radicals that can be generated by hydrogen abstraction from 1-propanol [40], as listed in Table 2. These reactions have been defined in the *pif.chem* file and the MP-CVT/SCT thermal rate constants for each channel have been fitted to the following expression [76]:

$$k = A \left(\frac{T}{T_R} \right)^n \exp \left[- \frac{E(T + T_0)}{R(T^2 + T_0^2)} \right] \quad (93)$$

where T_R is a reference temperature given by $T_R \equiv 300$ K, and A , E , n , and T_0 are fitting parameters (Listing E.1). These parameters were fitted to the MP-CVT/SCT thermal rate constants obtained in the temperature range 1000–2000 K. *Pilgrim* can also fit calculated rate constants to expressions other than Eq. (93), which in the *pif.kmc* file is referred as *analytic4*. The program can also use the numerical value of the thermal rate constants instead of analytical expressions. For more details we refer to the manual of the program.

The thermal rate constants can be specified in the forward direction (*fw*), in the backward direction (*bw*), or in both. Thus, for the H-migration reactions (R7, R9, R10, R12, R13 and

R14), the expressions for both the forward and backward rate constants are needed. Additionally, the KMC input file (*pif.kmc*) allows specifying the volume of the reaction vessel and the time units (microseconds in the example), as well as the initial populations of the reagents that are initially present. The default initial population is zero; therefore the user only needs to specify the nonzero initial populations. In the example, the only nonzero population is one million molecules of the $\text{CH}_3\text{CH}_2\dot{\text{C}}\cdot\text{HOH}$ radical. The command

```
pilgrim.py --kmc anaC1
```

runs the KMC algorithm for the simulation, where *anaC1* is the name given by the user to this case. An extract of the output is shown in Listing E.2.

It is possible to specify more than one simulation in the *pif.kmc* file. For instance, to run a simulation with the initial population just in the $\text{CH}_3\dot{\text{C}}\cdot\text{HCH}_2\text{OH}$ radical and at the temperatures indicated in the *pif.temp* file, the user should execute

```
pilgrim.py --kmc anaC2
```

If the label of the simulation is not included in the command, *Pilgrim* runs all the simulations included in the *pif.kmc* file.

4. Additional examples

In addition to the examples described above, a total of 11 fully commented worked examples are included in the manual of *Pilgrim*. These examples allow the user to explore most of the capabilities of the program. The corresponding output files for these examples are included with the documentation. Additional information is available in the manual.

5. Final remarks and future directions

Pilgrim can calculate thermal rate constants of reactions involving multiple conformations of reactants, transition states, and products by means of variational transition state theory (VTST) including multidimensional tunneling. *Pilgrim* can deal with more than one reaction in the same working directory, i.e., many elementary steps can be considered together. *Pilgrim* can also simulate the temporal evolution of the system with many elementary steps through a Kinetic Monte Carlo (KMC) simulation. Thus, it is possible to estimate the final product branching ratios of a proposed chemical mechanism.

An additional feature of the program not mentioned so far, but explained in the manual, is the possibility to perform dual-level calculations automatically. First, low-level calculations are carried out for the reaction of interest. Then single-point energy calculations of the reactants, transition structures, points along the MEP, and (optionally) products are performed at a higher level. Finally the low-level calculations are corrected with the high-level single point energies using the interpolated single-point energies (ISPE) algorithm [77].

Possibilities for future versions include pressure dependence, version 4 of the large curvature tunneling (LCG4) [78–80], approximation, the microcanonically optimized multidimensional tunneling method (μOMT) [14], and the least-action tunneling path method (LAT) [81–83].

6. Acknowledgments

The authors thank “Centro de Supercomputación de Galicia (CESGA)” for the use of their computational facilities. Financial support from the Consellería de Cultura, Educación e Ordenación Universitaria (Axuda para Consolidación e Estructuración de unidades de investigación competitivas do Sistema Universitario de Galicia, Xunta de Galicia ED431C 2017/17 & Centro singular de investigación de Galicia acreditación 2019-2022, ED431G 2019/03) and the European Regional Development Fund (ERDF) is gratefully acknowledged. D. F-C. thanks Xunta de Galicia for financial support through a postdoctoral grant. This work was supported in part by the U.S. Department of Energy, Office of Science, Office of Basic Energy Sciences under Award DE-SC0015997.

APPENDIXES

A. Selected program outputs of reactions R1h and R1d

Listing A.1: Extract of the help of the interactive menu of *Pilgrim*, which can be accessed by the `--input` option.

```
List of commands ($cmd) and variables ($var):
```

\$cmd\ \$var	struc	isomass	temp	chem	path	kmc	dlevel
help	x	x	x	x	x	x	x
ls	x	x	x	x	x	x	x
add		x+	x+	x+	x+	x+	x
mod	x+				x+	x+	
rm	x+	x	x+	x+	x+	x	x

```

x: the combination $cmd $var is available
+: the combination $cmd $var requires $values

Information about variables ($var):
```

\$var	addresses...	which contains...
struc	pif.struc	structures & isot. masses
isomass	pif.struc	structures & isot. masses
temp	pif.temp	temperatures
chem	pif.chem	reactions
path	pif.path & pif.calcs	MEP parameters
kmc	pif.kmc	variables in the KMC
dlevel	pif.dlevel	structures for high-level

Listing A.2: Species participating in reaction **R1h**; `m.form.` is the molecular formula; `num.ifreqs.` is the number of imaginary frequencies; `ch` is charge; `mtp` is multiplicity; `num.conf.` is the total number of conformations and total number of conformations discounting the conformational enantiomers (in parentheses); `iso.mod.` indicates if the species has a isotopic substitution; `num(minimum)` and `num(saddle)` refer to the number of minimum and transition state structures, respectively.

species name	m.form.	num.ifreqs.	ch	mtp	num.conf.	iso.mod.
CH3CH2O	C(2)H(5)O	0	0	2	1 (1)	none
CH3CH2OH	C(2)H(6)O	0	0	1	2 (2)	none
H	H	0	0	2	1 (1)	none
H2	H(2)	0	0	1	1 (1)	none
TSoh	C(2)H(7)O	1	0	2	2 (2)	none

```

* num(minimum) = 5 (5)
* num(saddle) = 2 (2)

```

Listing A.3: Same as Listing A.2. It should be notice that the number of total conformers was corrected after modifying the weights of the *gauche* conformers.

species name	m.form.	num.ifreqs.	ch	mtp	num.conf.	iso.mod.
--------------	---------	-------------	----	-----	-----------	----------

CH3CH2O	C(2)H(5)O	0	0	2	1 (1)	none
CH3CH2OH	C(2)H(6)O	0	0	1	3 (2)	none
H	H	0	0	2	1 (1)	none
H2	H(2)	0	0	1	1 (1)	none

TSoh	C(2)H(7)O	1	0	2	3 (2)	none

* num(minimum) = 6 (5)						
* num(saddle) = 3 (2)						

Listing A.4: List of all species as displayed by typing 'ls struc'. Species with isotopic substitutions are now included.

species name	m.form.	num.ifreqs.	ch	mtp	num.conf.	iso.mod.
CH3CH2O	C(2)H(5)O	0	0	2	1 (1)	none
CH3CH2OH	C(2)H(6)O	0	0	1	3 (2)	none
H	H	0	0	2	1 (1)	none
H2	H(2)	0	0	1	1 (1)	none
CH3CH2OD	C(2)H(6)O	0	0	1	3 (2)	D(9)
D	H	0	0	2	1 (1)	D(1)
D2	H(2)	0	0	1	1 (1)	D(all_H)

TSoh	C(2)H(7)O	1	0	2	3 (2)	none
TSod	C(2)H(7)O	1	0	2	3 (2)	D(9,10)

* num(minimum) = 11 (9)						
* num(saddle) = 6 (4)						

Listing A.5: Output from the *pfn.H2.slevel.txt* file. The translational, electronic, rotational, and vibrational partition functions were calculated using Eqs. (8), (9), (12), and (16), respectively. The total partition function was calculated using Eq. (7) with the HO approximation ($\lambda^{\text{ZPE}} = 1$).

```

-----
Analysis of STRUC: H2
-----

Pilgrim output file: 3-PLG_OUTPUT/pfn.H2.slevel.txt

Number of conformers: 1

V0 = electronic energy
V1 = electronic energy + zero-point energy (ZPE)

ZPE is calculated using scaled frequencies
Frequency scale factor: 1.00000

min(V0) = -1.11750590 hartree
min(V1) = -1.10501868 hartree

Relative energies (in kcal/mol):
-----
name | V0-min(V0) | V1-min(V1) | ZPE | mass (amu) | weight | PGS
-----
001 | 0.00 | 0.00 | 7.84 | 2.02 | 1 | Dinfv
-----

weight: equals 2 if the structure has a conformational enantiomer,
equals 1 otherwise
PGS : point group of symmetry

```

```

-----
Conformation: 001
-----
| Molecular formula      : H(2)
| Number of atoms       : 2
| Number of electrons   : 2
| Vibrational DOFs      : 1
| Charge                : 0
| Multiplicity          : 1
| Electronic energy (V0): -1.11750590 hartree
| Total mass [root]     : 2.0156 amu
| Total mass            : 2.0156 amu
| Point group symmetry  : Dinfv
| Rotational sym num    : 2
| Cartesian coordinates (Angstrom):
|   H   -0.356115   +0.000000   +0.000000   [ 1.008 amu]
|   H   +0.356115   +0.000000   +0.000000   [ 1.008 amu]
| Moments and product of inertia (au):
|       +1.664E+03
| Vibrational frequencies [1/cm] (scaled by 1.000):
|       5481.25
| Vibrational zero-point energies [kcal/mol]:
|       7.84
| Vibrational zero-point energy:      +0.01248722 hartree =
|                                       +7.84 kcal/mol =
|                                       +0.34 eV =
|                                       +2740.63 cm^-1
| V0 + zero-point energy   V1 =      -1.10501868 hartree
|
| Partition functions (pfns):
|-----|-----|-----|-----|-----|-----|
| T (K) | Qtr  | Qrot  | Qvib  | Qel   | Qtot
|-----|-----|-----|-----|-----|-----|
| 298.15 | 4.103E-01 | 1.571E+00 | 1.000E+00 | 1.000E+00 | 6.446E-01
|-----|-----|-----|-----|-----|-----|
| Qtr : translational pfn (in au)
| Qrot: rotational pfn (rigid-rotor)
| Qvib: vibrational pfn (harmonic-oscillator) relative to V1
| Qel : electronic pfn
| Qtot: total pfn per unit volume (in au)
|
| Both Qrot and Qtot include rotational symmetry number
|
| Gibbs free energy (hartree):
|-----|-----|-----|
| T (K) | V = 1 cm^3 | V = kbT/p0
|-----|-----|-----|
| 298.15 | -1.15858443 | -1.11643907
|-----|-----|-----|
| V : volume per molecule
| p0: 1bar
|

```

Listing A.6: Extract of the output from the *pfn.CH3CH2OH.slevel.txt* file showing the section associated with the MS-HO partition function.

Number of conformers: 3

```

VO = electronic energy
V1 = electronic energy + zero-point energy (ZPE)

ZPE is calculated using scaled frequencies
Frequency scale factor: 1.00000

min(V0) = -152.13306610 hartree
min(V1) = -152.03827812 hartree

Relative energies (in kcal/mol):
-----
name | V0-min(V0) | V1-min(V1) | ZPE   | mass (amu) | weight | PGS
-----
 001 |      0.00 |      0.00 | 59.48 |      46.04 |      2 |  C1
 002 |      0.25 |      0.19 | 59.42 |      46.04 |      1 |  Cs
-----

weight: equals 2 if the structure has a conformational enantiomer,
        equals 1 otherwise
PGS    : point group of symmetry
...
...
...
Total multi-structural HO pfn (QMS_HO) and Gibbs free energies (GFE):
-----
T (K) | QMS_HO | GFE [V = 1 cm^3] | GFE [V = kbT/p0]
-----
298.15 | 4.402E+06 | -152.10670228 | -152.06455692
-----

QMS_HO is calculated with regard to min(V1)

Individual contributions to the partition function:
-----
T (K) | 001 | 002
-----
298.15 | 0.726 | 0.274
-----

```

Listing A.7: Extract of the output *rcons.R1h.slevel.txt* file showing the energetics of the R1h reaction, its forward and backward equilibrium constants, TST thermal rate constants and free energies of activation.

```

Relative energies (kcal/mol):

V0(i) is the electronic energy of the i-th conformer
V1(i) = V0(i)+ZPE(i)
ZPE(i) is the harmonic oscillator ZPE of the i-th conformer

min{V0(i)} of reactants ==> V0 = -152.59964800 hartree
min{V1(i)} of reactants ==> V1 = -152.50486002 hartree

-----
SP                | V0(i)-V0 | V1(i)-V1 | weight
-----
CH3CH2OH.001+H.001 |      0.00 |      0.00 |      2
CH3CH2OH.002+H.001 |      0.25 |      0.19 |      1
-----
TSoh.001           |      8.78 |      7.04 |      2
TSoh.002           |      8.83 |      7.02 |      1
-----
CH3CH2O.001+H2.001 |     -39.07 |     -41.56 |      1

```

SP: stationary point

EQUILIBRIUM CONSTANT

- Keq : the equilibrium constant
- GFER : the Gibbs free energy of reaction (kcal/mol)
- R2P : from reactant(s) to product(s)
- P2R : from product(s) to reactant(s)

Keq(P2R) = 1/Keq(R2P)
GFER(P2R) = - GFER(R2P)

for V=1cm³ per molecule

T (K)	Keq (R2P)	Keq (P2R)	GFER (R2P)
298.15	+4.202E+30	+2.380E-31	-41.778

for V=kB*T/p0 per molecule, p0=1bar

T (K)	Keq (R2P)	Keq (P2R)	GFER (R2P)
298.15	+4.202E+30	+2.380E-31	-41.778

TRANSITION STRUCTURE CONTRIBUTIONS

The contribution of the j-th transition state conformer to the MS-TST rate constant is calculated as:

$$\chi_j^{\text{TST}} = w_j * (Q^{\{\text{RR-HO}\}}_j / Q^{\{\text{MS-HO}\}}) * \exp(-U_j/kB/T)$$

where

w_j : weight of j-th conformer (1 or 2)
Q^{RR-HO}_j: rigid-rotor harmonic-oscillator partition function
Q^{MS-HO}: multi-structural harmonic-oscillator partition function
U_j : relative energy with regard to the most stable conformer (considering the ZPE)

T (K)	Conf	chi_j TST
298.15	001	0.63749
	002	0.36251

FORWARD RATE CONSTANTS

- units: cm³/molecule/s

T (K)	TS	MS-TST
298.15	total	1.087E-16
	001	6.930E-17
	002	3.941E-17

FORWARD GIBBS FREE ENERGIES OF ACTIVATION (GFEA)

* GFEA = $-R T \ln(h k V^{-1} / k_B T)$
 - units: kcal/mol
 - reference volume: 1 cm³ per molecule

T (K)	MS-TST
298.15	39.232

* GFEA = $-R T \ln(h k V^{-1} / k_B T)$
 - units: kcal/mol
 - reference volume: $k_B T / p_0$ per molecule, with $p_0 = 1$ bar

T (K)	MS-TST
298.15	12.785

BACKWARD RATE CONSTANTS

- units: cm³/molecule/s

T (K)	TS	MS-TST
298.15	total	2.587E-47
	001	1.649E-47
	002	9.378E-48

BACKWARD GIBBS FREE ENERGIES OF ACTIVATION (GFEA)

* GFEA = $-R T \ln(h k V^{-1} / k_B T)$
 - units: kcal/mol

```

- reference volume: 1 cm^3 per molecule

-----
T (K)   |      MS-TST
-----
298.15  |      81.010
-----

* GFEA = -R T ln(h k V^-1 / kB T)
- units: kcal/mol
- reference volume: kB*T/p0 per molecule, with p0 = 1 bar

-----
T (K)   |      MS-TST
-----
298.15  |      54.563
-----

```

Listing A.8: *Gaussian* template inside the *pif.calcs* file, automatically generated from the input menu for TSoh species.

```

start_meppoint TSoh gaussian
%nproc=1
%mem=1GB
%chk=[Pilgrim_name].chk
#p hf/sto-3g
scf=verytight
NoSymm
[Pilgrim_gradhess]

Input file for MEP calculation

0 2
[Pilgrim_geometry]

end_meppoint

```

Listing A.9: Extract of the *pif.struc* file showing the specification of the internal coordinates for the **R1h** reaction.

```

start_ctc TSoh
root      TSoh
# conformers & anharmonicity
conformer 001 * 2 # 0.000 kcal/mol, C1
conformer 002 * 1 # 0.058 kcal/mol, Cs
# basic data
mformu    C(2)H(7)O
ch         0
mtp       2
type      1
freqscal  1.000
elestate  2 0.0000000000E+00
# internal coordinates
ics       1-2 2-3 2-4 2-5 3-6
ics       3-7 3-8 6-9 9-10
ics       1-2-3 1-2-4 1-2-5 2-3-6 2-3-7
ics       2-3-8 3-2-4 3-2-5 3-6-9 4-2-5
ics       6-3-7 6-3-8 7-3-8
ics       6=9=10
ics       1_3_4_2 1_3_5_2 1_4_5_2 2_6_7_3 2_6_8_3

```

```

ics      2_7_8_3  3_4_5_2  6_7_8_3
ics      1-2-3-6  1-2-3-7  1-2-3-8  2-3-6-9  4-2-3-6
ics      4-2-3-7  4-2-3-8  5-2-3-6  5-2-3-7  5-2-3-8
ics      7-3-6-9  8-3-6-9
end_ctc

```

Listing A.10: Extract of the *path.TSoh.001.slevel.txt* file listing the reference energy, the progression along the MEP, the total energy and the relative energy with respect to the reference energy.

Reference energy (Eref) set to: -152.599648 hartree

```

-----
s (bohr) | E (hartree) | E-Eref (hartree) | E-Eref (kcal/mol)
-----
-2.0000 | -152.5992080 | +0.0004400 | +0.276
-1.9000 | -152.5990964 | +0.0005516 | +0.346
...
-0.2000 | -152.5879146 | +0.0117334 | +7.363
-0.1000 | -152.5864887 | +0.0131593 | +8.258
-0.0000 | -152.5856639 | +0.0139841 | +8.775
+0.1000 | -152.5872737 | +0.0123743 | +7.765
+0.2000 | -152.5930760 | +0.0065720 | +4.124
...
+1.9000 | -152.6572472 | -0.0575992 | -36.144
+2.0000 | -152.6579748 | -0.0583268 | -36.601
-----

```

Listing A.11: Extract of the *path.TSoh.001.slevel.txt* file listing the potential along the MEP and the ZPE in Cartesian (cc) and internal (ic) coordinates; The vibrational adiabatic potential V_a^G and the reference energy plus V_a^G are also listed.

```

-----
s (bohr) | V_MEP | ZPE(cc) | ZPE(ic) | VaG | | Eref + VaG (au)
-----
-2.000 | +0.276 | 59.478 | 59.662 | +59.938 || -152.50413097
-1.900 | +0.346 | 59.475 | 59.683 | +60.029 || -152.50398513
...
-0.200 | +7.363 | 58.221 | 59.469 | +66.832 || -152.49314487
-0.100 | +8.258 | 57.723 | 58.611 | +66.869 || -152.49308555
-0.000 | +8.775 | 57.742 | 57.742 | +66.517 || -152.49364627
+0.100 | +7.765 | 57.945 | 57.473 | +65.238 || -152.49568502
+0.200 | +4.124 | 58.011 | 57.475 | +61.599 || -152.50148312
...
+1.900 | -36.144 | 58.047 | 58.781 | +22.637 || -152.56357374
+2.000 | -36.601 | 57.913 | 58.552 | +21.952 || -152.56466598
-----
-0.145 | Maximum of VaG (VAG) | | +66.907 || -152.49302569
-----

```

Listing A.12: Extract of the *path.TSoh.001.slevel.txt* file indicating the location of s_*^{CVT} , and the values of Γ^{CVT} and $\Delta\Delta G_{var}^0$ (DDGFE); the TST/CAG and the CVT/CAG transmission coefficients are also listed.

```

-----
T (K) | s_CVT | Gamma^CVT | DDGFE
-----
298.15 | -0.1316 | 5.7945E-01 | 0.3233
-----
...
-----
T (K) | VAG-VaG(s=0) | TST/CAG | | VAG-VaG(s_CVT) | CVT/CAG
-----

```

```
-----
298.15 |          0.3894 | 5.183E-01 ||          0.0035 | 9.941E-01
-----
Energy differences in kcal/mol
```

Listing A.13: Extract of the *path.TSoh.001.slevel.txt* file listing data related to the tunneling calculations; see text.

```
Summary table
- Progress along the path (s) in bohr
- Vibrationally adiabatic potential (VaG) in kcal/mol
- kappa (curvature) in bohr^-1
- Turning point (turnpoint) in bohr
- Effective mass (mueff) in a.u.
-----
  s | VaG | kappa | turnpoint | mueff | mueff/mu
-----
-2.000 | +59.938 | +3.43E-01 | 0.25599 | 1525.3355 | 0.8368
-1.900 | +60.029 | +3.34E-01 | 0.24867 | 1538.6496 | 0.8441
...
-0.200 | +66.832 | +2.09E+00 | 0.19125 | 713.1338 | 0.3912
-0.100 | +66.869 | +3.60E+00 | 0.21423 | 228.1790 | 0.1252
-0.000 | +66.517 | +2.23E+00 | 0.23910 | 674.8725 | 0.3702 **
+0.100 | +65.238 | +8.55E-01 | 0.26396 | 1121.5660 | 0.6153
+0.200 | +61.599 | +5.56E-01 | 0.26498 | 1330.8187 | 0.7301
...
+1.900 | +22.637 | +5.24E-01 | 0.56890 | 931.1407 | 0.5108
+2.000 | +21.952 | +7.43E-01 | 0.58078 | 647.0376 | 0.3550
-----
** kappa, turnpoint and mueff were interpolated

Transmission probabilities will be calculated between E0 and VAG:
E0 = 59.4804 kcal/mol
VAG = 66.9065 kcal/mol

Transmission probabilities for Kappa^SAG calculation:
-----
  E [kcal/mol] | P^ZCT(E) | P^SCT(E) | Classical turning
                |          |          | points [bohr]
-----
  59.4804 | 7.797e-09 | 1.128e-07 | [-2.000,+0.239] L
  59.4820 | 7.847e-09 | 1.135e-07 | [-2.000,+0.239] L
  59.4891 | 8.060e-09 | 1.163e-07 | [-2.000,+0.239] L
  ...
  66.8851 | 4.912e-01 | 4.960e-01 | [-0.175,-0.111]
  66.8978 | 4.964e-01 | 4.984e-01 | [-0.164,-0.124]
  66.9049 | 4.993e-01 | 4.997e-01 | [-0.153,-0.136]
-----

Number of tunneling energies: 81

WARNING! Some tunneling probabilities are not converged:
* 'L' --> at the left-side of VaG(s).
* 'R' --> at the right-side of VaG(s).
* 'B' --> at both sides of VaG(s).
This fact may lack of importance if the temperature
is high enough so these probabilities do not play
any role.
```

```

ZCT transmission coefficient:
-----
  T (K) | %I1 | %I2 | Kappa^ZCT | RTE
-----
  298.15 | 91.72 | 8.28 | 8.320E+00 | 64.690
-----
RTE: Representative Tunneling Energy (in kcal/mol)
%I1: contribution of tunneling
%I2: contribution of non-classical reflection
++ : indicates that QRC was used at the given temperature
** : indicates that RTE is close to E0 (less than 1.5 kcal/mol)

SCT transmission coefficient:
-----
  T (K) | %I1 | %I2 | Kappa^SCT | RTE
-----
  298.15 | 97.75 | 2.25 | 2.768E+01 | 63.568
-----
RTE: Representative Tunneling Energy (in kcal/mol)
%I1: contribution of tunneling
%I2: contribution of non-classical reflection
++ : indicates that QRC was used at the given temperature
** : indicates that RTE is close to E0 (less than 1.5 kcal/mol)
...

SUMMARY OF CALCULATED COEFFICIENTS:
-----
  T (K) | Gamma | Kappa | Kappa | Kappa | Kappa
        | CVT   | ZCT   | SCT   | TST/CAG | CVT/CAG
-----
  298.15 | 5.7945E-01 | 8.3199E+00 | 2.7682E+01 | 5.1827E-01 | 9.9408E-01
-----

```

Listing A.14: Extract of the *rcons.Rlh.slevel.txt* file listing various multipath transmission coefficients which correct the MS-TST thermal rate constant.

```

-----
TOTAL TRANSMISSION COEFFICIENTS
-----

The averaged transmission coefficient
for a given method (X) is:

  <gamma>^X = k^X / k^TST
...

-----
  T (K) | Conf | gamma | gamma | gamma | gamma | gamma
        |     | TST/ZCT | TST/SCT | CVT | CVT/ZCT | CVT/SCT
-----
  298.15 | all | 4.265E+00 | 1.403E+01 | 5.870E-01 | 4.750E+00 | 1.563E+01
        | 001 | 4.312E+00 | 1.435E+01 | 5.794E-01 | 4.792E+00 | 1.595E+01
        | 002 | 4.183E+00 | 1.348E+01 | 6.002E-01 | 4.676E+00 | 1.507E+01
-----

```

Listing A.15: Extract of the *rcons.Rlh.slevel.txt* file with the forward rate constants calculated by different methods. Rate constants based on the ZCT transmission coefficient have been omitted in this listing for a better presentation of data.

```

-----
FORWARD RATE CONSTANTS
-----

- units: cm^3/molecule/s

-----
T (K) | TS | MS-TST | MS-TST/SCT | MS-CVT | MS-CVT/SCT
-----
298.15 | total | 1.087E-16 | 1.560E-15 | 6.299E-17 | 1.733E-15
      | 001 | 6.930E-17 | 9.942E-16 | 4.015E-17 | 1.105E-15
      | 002 | 3.941E-17 | 5.653E-16 | 2.283E-17 | 6.283E-16
-----

T (K) | TS | MS-TST | MP-TST/SCT | MP-CVT | MP-CVT/SCT
-----
298.15 | total | 1.087E-16 | 1.525E-15 | 6.381E-17 | 1.699E-15
      | 001 | 6.930E-17 | 9.942E-16 | 4.015E-17 | 1.105E-15
      | 002 | 3.941E-17 | 5.311E-16 | 2.365E-17 | 5.937E-16
-----

```

Listing A.16: *Pilgrim* menu for the --kies option. In blue, information provided by the user.

```

Available reactions
-----

Mmethods: the number of methods the rate constant was calculated with

-----
reaction | dir | keyword | Nmethods
-----
R1d | fw | R1d.fw | 11
R1d | bw | R1d.bw | 11
-----
R1h | fw | R1h.fw | 11
R1h | bw | R1h.bw | 11
-----

Reactions are selected as in the 'keyword' column ($reaction.$dir)

Introduce reactions without/with isotopic substitution(s)
Type 'end()' or 'exit()' to finish
>> without: R1h.fw
>> with : R1d.fw

```

Listing A.17: Translational, rovibrational and torsional anharmonic contributions to the KIE.

```

Contributions to the total KIE (method-independent):

-----
T (K) | kie_tr | kie_rv | kie_tor
-----
298.15 | 2.741 | 1.718 | 1.000
-----

```

Listing A.18: Variational-tunneling contribution to the KIE and the total KIE.

Total KIE and vtun contribution (method-dependent):

T (K)	method	kie_vtun	kie_tot
298.15	MS-TST	-	4.709
	MS-TST/ZCT	1.556	7.329
	MS-TST/SCT	1.879	8.848
	MS-CVT	0.673	3.170
	MS-CVT/ZCT	1.659	7.811
	MS-CVT/SCT	2.002	9.430
	MP-TST/ZCT	1.547	7.286
	MP-TST/SCT	1.871	8.809
	MP-CVT	0.679	3.197
	MP-CVT/ZCT	1.652	7.782
	MP-CVT/SCT	1.998	9.408

Listing A.19: Individual transition-structure contributions to the KIE. Notice that `kie#_j` refers to $\tilde{\eta}_j$.

Contribution of each transition structure to KIE using MP-CVT/SCT:

T (K)	SP	rv,j	vtun,j	P_j,D	P_j,H	kie_j	kie#_j
298.15	001	1.713	2.002	0.651	0.650	9.401	6.120
	002	1.728	1.990	0.349	0.350	9.421	3.288

B. Page-McIver algorithm

This method uses a local quadratic approximation at a given point and starts from an equation equivalent to Eq. (33):

$$\frac{d\mathbf{x}}{d\zeta} = -\hat{\mathbf{G}}(\mathbf{x}) \quad (\text{B.1})$$

where ζ is a progress variable along the path, which is related to s by

$$\frac{ds}{d\zeta} = \sqrt{\frac{d\mathbf{x}^\dagger d\mathbf{x}}{d\zeta d\zeta}} \quad (\text{B.2})$$

A local quadratic approximation at a given point \mathbf{x}_n of the MEP at which the gradient and the Hessian are available allows us to write

$$\hat{\mathbf{G}}(\mathbf{x}) = \hat{\mathbf{G}}(\mathbf{x}_n) + \mathbf{F}(\mathbf{x}_n)(\mathbf{x} - \mathbf{x}_n) \quad (\text{B.3})$$

By substituting Eq. (B.3) into Eq. (B.1) the following equation is obtained:

$$\frac{d\mathbf{x}}{d\zeta} = -\hat{\mathbf{G}}(\mathbf{x}_n) - \mathbf{F}(\mathbf{x}_n)(\mathbf{x} - \mathbf{x}_n) \quad (\text{B.4})$$

whose integration gives the steepest descent path. Thus, the next step along the MEP is given by:

$$\mathbf{x}_{n+1} = \mathbf{x}_n + \mathbf{A}_n(\zeta)\mathbf{v}_n \quad (\text{B.5})$$

where

$$\mathbf{A}_n(\zeta) = \mathbf{U}_n \mathbf{M}_n(\zeta) \mathbf{U}_n^\dagger \quad (\text{B.6})$$

and $\mathbf{M}_n(\zeta)$ is a diagonal matrix whose elements are:

$$M_{ii}(\zeta) = [\exp(-\alpha_{n,ii}\zeta) - 1] / \alpha_{n,ii} \quad (\text{B.7})$$

and the values $\alpha_{n,ii}$ are the eigenvalues obtained from the diagonalization of the Hessian at \mathbf{x}_n :

$$\alpha_n = \mathbf{U}_n^\dagger \mathbf{F}_n \mathbf{U}_n \quad (\text{B.8})$$

Taking into account these equations, Eq. (B.2) is rewritten as:

$$\frac{ds}{d\zeta} = \left(\sum_{i=1}^{3N} h_i^2 \exp(-2\alpha_{n,ii}\zeta) \right)^{-1} \quad (\text{B.9})$$

where

$$\mathbf{h}_n = \mathbf{U}_n^\dagger \mathbf{G}_n \quad (\text{B.10})$$

The value of ζ can be found iteratively by integration of Eq. (B.9)

$$\delta s = \int_0^\zeta d\zeta' \left(\sum_{i=1}^{3N} h_i^2 \exp(-2\alpha_{n,ii}\zeta') \right)^{-1} \quad (\text{B.11})$$

where $\delta s = s_{n+1} - s_n$ is the step size.

C. Details on the SCT approximation

In the small-curvature approximation (SCT) the action integral $\theta(E)$ is

$$\theta(E) = h^{-1} \int_{s_<(E)}^{s_>(E)} ds \left\{ 2\mu_{\text{eff}}(s) [V_a^G(s) - E] \right\}^{\frac{1}{2}} \quad (\text{C.1})$$

where $s_<(E)$ and $s_>(E)$ are the left and right classical turning points at which

$$V_a^G(s) = E \quad (\text{C.2})$$

In some cases (when the V_a^G curve has more than one local maximum) there are more than two classical turning points, so we have to find all the roots of Eq. (C.2). For instance in the case that there are two additional roots s_1 and s_2 between $s_<$ and $s_>$ where $s_< < s_1 < s_2 < s_>$ the action integral is

$$\theta(E) = h^{-1} \left\{ \int_{s_<(E)}^{s_1(E)} ds \left\{ 2\mu_{\text{eff}}(s) [V_a^G(s) - E] \right\}^{\frac{1}{2}} + \int_{s_2(E)}^{s_>(E)} ds \left\{ 2\mu_{\text{eff}}(s) [V_a^G(s) - E] \right\}^{\frac{1}{2}} \right\} \quad (\text{C.3})$$

The action integral is evaluated over the classically forbidden region(s), that is, for regions in which the total energy is lower than the effective potential, which is V_a^G . The coupling between the reaction coordinate and the rest of degrees of freedom is included in the effective mass $\mu_{\text{eff}}(s)$; if the coupling is neglected, i.e., $\mu_{\text{eff}}(s) = \mu$, we have the zero-curvature tunneling (ZCT)

approximation, which approximates the tunneling path as coinciding with the MEP and neglects its curvature. When coupling is included $\mu_{\text{eff}}(s) \leq \mu$, so the action integral is smaller and the tunneling probability is larger. In SCT, the effective mass is written as

$$\mu_{\text{eff}}^{\text{SC}}/\mu = \min \left\{ \begin{array}{l} \exp \left\{ -2\bar{a}(s) - [\bar{a}(s)]^2 + (d\bar{t}/ds)^2 \right\} \\ 1 \end{array} \right\} \quad (\text{C.4})$$

where

$$\bar{a} = |\kappa(s)\bar{t}(s)| \quad (\text{C.5})$$

in which $\kappa(s)$ is the reaction-path curvature

$$\kappa(s) = \left\{ \sum_{m=1}^{F-1} [B_{mF}(s)]^2 \right\}^{1/2} \quad (\text{C.6})$$

and $\bar{t}(s)$ is the turning point

$$\bar{t} = \left[\frac{\hbar}{\mu\bar{\omega}(s)} \right]^{\frac{1}{2}} = \left(\sum_{m=1}^{F-1} \left[\frac{B_{mF}(s)}{\kappa(s)} \right]^2 [t_m(s)]^{-4} \right)^{-\frac{1}{4}} \quad (\text{C.7})$$

of a harmonic potential of frequency

$$\bar{\omega} = \left(\sum_{m=1}^{F-1} \left[\frac{B_{mF}(s)}{\kappa(s)} \omega_m(s) \right]^2 \right)^{\frac{1}{2}} \quad (\text{C.8})$$

which leads to a harmonic expansion of the potential about the MEP

$$V = V_{\text{MEP}}(s) + \frac{1}{2}\mu[\bar{\omega}(s)]^2 u_1^2 \quad (\text{C.9})$$

in which one axis of coordinates u_1 coincides with the vector that includes the couplings between the reaction coordinate and the rest of degrees of freedom $\mathbf{B}_F(s)$, so the coupling is zero along the other axes $u_2 \dots u_{F-1}$. In Eq (C.7), the individual turning points $t_m(s)$ are given by

$$t_m(s) = \pm \left[\frac{\hbar}{\mu\omega_m(s)} \right]^{\frac{1}{2}} \quad (\text{C.10})$$

and the last term in the rhs of Eq. (C.4) is calculated using central-finite differences

$$\left(\frac{d\bar{t}}{ds} \right)^2 = \sum_{m=1}^{F-1} \left(\frac{dt_m(s)}{ds} \right)^2 = \sum_{m=1}^{F-1} \left(\frac{t_m(s + \delta s_H) - t_m(s - \delta s_H)}{2\delta s_H} \right)^2 \quad (\text{C.11})$$

with a step size given by $\delta s_H = N_H \delta s$, where N_H is the steps along the MEP between a Hessian calculations, as specified in Eq. 44.

The effective mass at the transition state, $\mu_{\text{eff}}(s = 0)$, is linearly interpolated using the two closest locations that have a Hessian available:

$$\mu_{\text{eff}}(s = 0) = \frac{1}{2} [\mu_{\text{eff}}(s = -\delta s_H) + \mu_{\text{eff}}(s = +\delta s_H)] \quad (\text{C.12})$$

The tunneling transmission probabilities are calculated by Eq. (55) for energies between E_0 and V^{AG} and the action integral is evaluated from Eq. (C.1) using Gauss-Legendre quadrature. For the ZCT transmission probabilities, $\mu_{\text{eff}}(s)$ is set equal to μ , whereas for the SCT ones the effective mass is the one calculated by Eqs. (C.4) and (C.12). The classical turning points are also indicated; these are the points that satisfy Eq. (C.2) at the energy for which the tunneling probability is being calculated.

D. Use of internal coordinates along the MEP

Curvilinear coordinates q can be written as a power series of displacements in Cartesian coordinates

$$q_i \simeq \sum_j^{3N} B_{ij} (R_j - R_j^0) + \frac{1}{2} \sum_j^{3N} \sum_k^{3N} C_{jk}^i (R_j - R_j^0) (R_k - R_k^0) \quad (\text{D.1})$$

where higher-order terms than the second are neglected. The superscript zero denotes a reference geometry, which in this case would be a point on the MEP at location s . In this section we suppress the dependence of all quantities on s to simplify the equations.

The subscript i runs over the F_{curv} internal coordinates, which in the redundant case is greater than $3N - 6$. The elements of the \mathbf{B} and \mathbf{C} Wilson matrices are given by:

$$B_{ij} = \left(\frac{\partial q_i}{\partial R_j} \right) \Big|_{\{R_j\}=\{R_j^0\}} \quad (\text{D.2})$$

and

$$C_{ij}^i = \left(\frac{\partial q_i}{\partial R_j \partial R_k} \right) \Big|_{\{R_k\}=\{R_k^0\}} \quad (\text{D.3})$$

Once those elements are calculated, the next step is to obtain the \mathbf{G}^{W} Wilson matrix

$$\mathbf{G}^{\text{W}} = \mathbf{B} \mathbf{u} \mathbf{B}^\dagger \quad (\text{D.4})$$

where \mathbf{u} is a $3N \times 3N$ diagonal matrix having as elements the reciprocal of the atomic masses. Next the $\mathbf{G}^{\text{W-}}$ matrix is obtained

$$\mathbf{G}^{\text{W-}} = (\mathbf{K} \mathbf{K}') \begin{pmatrix} \mathbf{\Gamma}^{-1} & 0 \\ 0 & 0 \end{pmatrix} \begin{pmatrix} \mathbf{K}^\dagger \\ (\mathbf{K}')^\dagger \end{pmatrix} \quad (\text{D.5})$$

where \mathbf{K} and \mathbf{K}' contain the eigenvectors associated with the nonzero and zero eigenvalues, respectively, and $\mathbf{\Gamma}$ contains the nonzero eigenvalues. The inverse of the \mathbf{B} matrix is built as

$$\mathbf{A} = \mathbf{u} \mathbf{B}^\dagger \mathbf{G}^{\text{W-}} \quad (\text{D.6})$$

Using Eq. (D.6) it is possible to obtain the gradient and the Hessian in redundant internal coordinates (\mathbf{g} and \mathbf{f} , respectively):

$$\mathbf{g} = \mathbf{A}^\dagger \mathbf{G} \quad (\text{D.7})$$

$$\mathbf{f} = \mathbf{A}^\dagger \mathbf{F} \mathbf{A} - \sum_i^{F_{\text{curv}}} g_i \mathbf{A}^\dagger \mathbf{C}^i \mathbf{A} \quad (\text{D.8})$$

From \mathbf{G}^W and \mathbf{G}^{W-} the projector

$$\mathbf{P} = \mathbf{G}^W \mathbf{G}^{W-} \quad (\text{D.9})$$

transforms the redundant internal gradient and Hessian into the non-redundant gradient ($\tilde{\mathbf{g}}$) and Hessian ($\tilde{\mathbf{f}}$)

$$\tilde{\mathbf{g}} = \mathbf{P} \mathbf{g} \quad (\text{D.10})$$

$$\tilde{\mathbf{f}} = \mathbf{P} \mathbf{f} \mathbf{P} \quad (\text{D.11})$$

The reaction coordinate is projected using the projector

$$\mathbf{p} = \frac{\tilde{\mathbf{g}} \tilde{\mathbf{g}}^\dagger}{\tilde{\mathbf{g}}^\dagger [\mathbf{B} \mathbf{u} \mathbf{B}^\dagger] \tilde{\mathbf{g}}} \quad (\text{D.12})$$

leading to the orthogonal $(3N - 7) \times (3N - 7)$ Hessian matrix

$$\tilde{\mathbf{f}}^{\text{p}} = \left\{ 1 - \mathbf{p} [\mathbf{B} \mathbf{u} \mathbf{B}^\dagger] \right\} \tilde{\mathbf{f}} \left\{ 1 - [\mathbf{B} \mathbf{u} \mathbf{B}^\dagger] \mathbf{p} \right\} \quad (\text{D.13})$$

Finally, this Hessian matrix is diagonalized:

$$\mathbf{G}^W \tilde{\mathbf{f}}^{\text{p}} \mathbf{L}^W = \mathbf{L}^W \mathbf{\Lambda} \quad (\text{D.14})$$

and the transverse vibrational frequencies are given by

$$\omega_m = \sqrt{\Lambda_{mm}} \quad (\text{D.15})$$

The eigenvectors \mathbf{L}^W are transformed into mass-scaled Cartesian displacement eigenvectors \mathbf{L} because the latter are needed to calculate the curvature coupling elements needed for the SCT calculation. To accomplish this we first normalize \mathbf{L}^W by:

$$\hat{\mathbf{L}}^W = \mathbf{L}^W \mathbf{W} \quad (\text{D.16})$$

where

$$W_{ij} = \sqrt{c_{ij}} \delta_{ij} \quad (\text{D.17})$$

$$\mathbf{c} = (\mathbf{L}^W)^{-1} \mathbf{G}^W \left[(\mathbf{L}^W)^{-1} \right]^\dagger \quad (\text{D.18})$$

The $\hat{\mathbf{L}}^W$ eigenvectors are used to obtain the Cartesian displacement normal-mode eigenvectors by

$$\chi = \mathbf{A} \hat{\mathbf{L}}^W \quad (\text{D.19})$$

and the elements of the mass-scaled Cartesian displacement eigenvectors are given by

$$L_{i,j} = \frac{(m_i/\mu)^{1/2} \chi_{ij}}{\left[\sum_k (m_k/\mu) \chi_{kj}^2 \right]^{1/2}} = \frac{m_i^{1/2} \chi_{ij}}{\left[\sum_k m_k \chi_{kj}^2 \right]^{1/2}} \quad (\text{D.20})$$

E. Selected program outputs for the decomposition of 1-propanol

Listing E.1: Extract of the *kmc.pif* file showing the input for the decomposition mechanism of the radicals produced by hydrogen abstraction from 1-propanol.

```

start_kmc anaC1
# KMC Parameters
psteps      10000      # print data each nstp steps
volume      1.00E+00    # simulation volume (cm^3)
timeunits   mcs        # units for time variable

# Initial (non-zero) populations (number of molecules)
pop0(nPrOH_C1) 1.00e+06

# Selection of the rate constant to use. Parameters: A, E, n, TR, T0
k(R01.fw) analytic4 2.7907E+14 1.1039E+04 -4.6290E-01 3.00E+02 1.3069E-03
...
k(R16.fw) analytic4 9.9840E+12 1.4452E+04 -2.3272E-03 3.00E+02 6.6047E-03
end_kmc

start_kmc anaC2
# KMC Parameters
psteps      10000      # print data each nstp steps
volume      1.00E+00    # simulation volume (mL)
timeunits   ps         # units for time variable

# Initial (non-zero) populations (number of molecules)
pop0(nPrOH_C2) 1.00e+06

# Selection of the rate constant to use. Parameters: A, E, n, TR, T0
k(R01.fw) analytic4 2.7907E+14 1.1039E+04 -4.6290E-01 3.00E+02 1.3069E-03
...
k(R16.fw) analytic4 9.9840E+12 1.4452E+04 -2.3272E-03 3.00E+02 6.6047E-03
end_kmc
...

```

Listing E.2: Extract of the *kmc.anaC1.slevel.txt* file which lists the total simulation time and the ratio of the final population of each species to the initial population of $\text{CH}_3\text{CH}_2\text{C}^*\text{HOH}$

```

-----
Simulation time in mcs
-----

-----
T (K) | sim. time
-----
1000.00 | 1.83E+00
1500.00 | 3.59E-03
2000.00 | 1.49E-04
-----

-----
Final ratios (pop(i)/POPO)
-----

-----
T (K) | CH2CH2 | CH2CH3 | CH2CHCH3 | CH3 | H
-----
1000.00 | 0.001 | 0.035 | 0.002 | 0.734 | 0.188
1500.00 | 0.002 | 0.028 | 0.005 | 0.656 | 0.268

```

```
2000.00 | 0.002 | 0.023 | 0.006 | 0.587 | 0.332
```

```
...
```

```
-----  
T (K) | OCH2 | OCHCH2CH3 | OH | nPrOH_C1 | nPrOH_C2  
-----  
1000.00 | 0.035 | 0.160 | 0.002 | 0.040 | 0.000  
1500.00 | 0.028 | 0.216 | 0.005 | 0.041 | 0.001  
2000.00 | 0.023 | 0.258 | 0.006 | 0.044 | 0.005  
-----
```

```
...
```

References

- [1] M. J. Frisch, G. W. Trucks, H. B. Schlegel, G. E. Scuseria, M. A. Robb, J. R. Cheeseman, J. A. Montgomery Jr., T. Vreven, K. N. Kudin, J. C. Burant, J. M. Millam, S. S. Iyengar, J. Tomasi, V. Barone, B. Mennucci, M. Cossi, G. Scalmani, N. Rega, G. A. Petersson, H. Nakatsuji, M. Hada, M. Ehara, K. Toyota, R. Fukuda, J. Hasegawa, M. Ishida, T. Nakajima, Y. Honda, O. Kitao, H. Nakai, M. Klene, X. Li, J. E. Knox, H. P. Hratchian, J. B. Cross, C. Adamo, J. Jaramillo, R. Gomperts, R. E. Stratmann, O. Yazyev, A. J. Austin, R. Cammi, C. Pomelli, J. W. Ochterski, P. Y. Ayala, K. Morokuma, G. A. Voth, P. Salvador, J. J. Dannenberg, V. G. Zakrzewski, S. Dapprich, A. D. Daniels, M. C. Strain, O. Farkas, D. K. Malick, A. D. Rabuck, K. Raghavachari, J. B. Foresman, J. V. Ortiz, Q. Cui, A. G. Baboul, S. Clifford, J. Cioslowski, B. B. Stefanov, G. Liu, A. Liashenko, P. Piskorz, I. Komaromi, R. L. Martin, D. J. Fox, T. Keith, M. A. Al-Laham, C. Y. Peng, A. Nanayakkara, M. Challacombe, P. M. W. Gill, B. Johnson, W. Chen, M. W. Wong, C. Gonzalez, J. A. Pople, Gaussian03, Gaussian, Inc., Pittsburgh PA, (2003).
- [2] M. J. Frisch, G. W. Trucks, H. B. Schlegel, G. E. Scuseria, M. A. Robb, J. R. Cheeseman, G. Scalmani, V. Barone, B. Mennucci, G. A. Petersson, H. Nakatsuji, M. Caricato, X. Li, H. P. Hratchian, A. F. Izmaylov, J. Bloino, G. Zheng, J. L. Sonnenberg, M. Hada, M. Ehara, K. Toyota, R. Fukuda, J. Hasegawa, M. Ishida, T. Nakajima, Y. Honda, O. Kitao, H. Nakai, T. Vreven, J. A. Montgomery Jr., J. E. Peralta, F. Ogliaro, M. Bearpark, J. J. Heyd, E. Brothers, K. N. Kudin, V. N. Staroverov, R. Kobayashi, J. Normand, K. Raghavachari, A. Rendell, J. C. Burant, S. S. Iyengar, J. Tomasi, M. Cossi, N. Rega, J. M. Millam, M. Klene, J. E. Knox, J. B. Cross, V. Bakken, C. Adamo, J. Jaramillo, R. Gomperts, R. E. Stratmann, O. Yazyev, A. J. Austin, R. Cammi, C. Pomelli, J. W. Ochterski, R. L. Martin, K. Morokuma, V. G. Zakrzewski, G. A. Voth, P. Salvador, J. J. Dannenberg, S. Dapprich, A. D. Daniels, O. Farkas, J. B. Foresman, J. V. Ortiz, J. Cioslowski, D. J. Fox, *Gaussian 09*, Gaussian, Inc., Wallingford CT, (2009).
- [3] M. J. Frisch, G. W. Trucks, H. B. Schlegel, G. E. Scuseria, M. A. Robb, J. R. Cheeseman, G. Scalmani, V. Barone, G. A. Petersson, H. Nakatsuji, X. Li, M. Caricato, A. V. Marenich, J. Bloino, B. G. Janesko, R. Gomperts, B. Mennucci, H. P. Hratchian, J. V. Ortiz, A. F. Izmaylov, J. L. Sonnenberg, D. Williams-Young, F. Ding, F. Lipparini, F. Egidi, J. Goings, B. Peng, A. Petrone, T. Henderson, D. Ranasinghe, V. G. Zakrzewski, J. Gao, N. Rega, G. Zheng, W. Liang, M. Hada, M. Ehara, K. Toyota, R. Fukuda, J. Hasegawa, M. Ishida, T. Nakajima, Y. Honda, O. Kitao, H. Nakai, T. Vreven, K. Throssell, J. A. Montgomery Jr., J. E. Peralta, F. Ogliaro, M. J. Bearpark, J. J. Heyd, E. N. Brothers, K. N. Kudin, V. N. Staroverov, T. A. Keith, R. Kobayashi, J. Normand, K. Raghavachari, A. P. Rendell, J. C. Burant, S. S. Iyengar, J. Tomasi, M. Cossi, J. M. Millam, M. Klene, C. Adamo, R. Cammi, J. W. Ochterski, R. L. Martin, K. Morokuma, O. Farkas, J. B. Foresman, D. J. Fox, *Gaussian 16*, Revision A-03, Gaussian, Inc., Wallingford CT, (2016).
- [4] F. Neese, The ORCA program system, *Wiley Interdiscip. Rev. Comput. Mol. Sci.* 2 (2011) 73–78.
- [5] D. G. Truhlar, B. C. Garrett, Variational transition state theory, *Acc. Chem. Res.* 13 (1980) 440–448.
- [6] D. G. Truhlar, A. D. Isaacson, B. C. Garrett, Generalized transition state theory, in: M. Baer (Ed.), *Theory of chemical reaction dynamics*, Vol. 4, CRC, Boca Raton, FL, 1985, pp. 65–137.
- [7] D. G. Truhlar, A. D. Isaacson, B. C. Garrett, Transition state theory, in: P. v. R. Schleyer, N. L. Allinger, T. Clark, J. Gasteiger, P. A. Kollman, H. F. S. III (Eds.), *Encyclopedia of Computational Chemistry*, Vol. 5, John Wiley & Sons, Chichester, UK, 1998, pp. 3094–3104.
- [8] D. G. Truhlar, Variational transition state theory and multidimensional tunneling for simple and complex reactions in the gas phase, solids, liquids, and enzymes, in: M. D. A. Kohen, H.-H. Limbach (Eds.), *Isotope Effects in Chemistry and Biology*, CRC Press, 2005, pp. 579–619.
- [9] D.-G. Truhlar, B.-C. Garrett, Variational transition state theory in the treatment of hydrogen transfer reactions, in: J. T. Hynes, J. P. Klinman, H.-H. Limbach, R. L. Schowen (Eds.), *Hydrogen-Transfer Reactions*, Vol. 2, Wiley-VCH, Weinheim, Germany, 2007, pp. 833–874.
- [10] A. Fernández-Ramos, A. Ellingson, B. C. Garrett, D. G. Truhlar, Variational transition state theory, *Rev. Comput. Chem.* 23 (2007) 125–262.
- [11] J. L. Bao, D. G. Truhlar, Variational transition state theory: theoretical framework and recent developments, *Chem. Soc. Rev.* 46 (2017) 7548–7596.
- [12] K. K. Baldrige, M. S. Gordon, R. Steckler, D. G. Truhlar, Ab initio reaction paths and direct dynamics calculations, *J. Phys. Chem.* 93 (1989) 5107–5119.
- [13] A. González-Lafont, T. N. Truong, D. G. Truhlar, Direct dynamics calculations with NDDO (neglect of diatomic differential overlap) molecular orbital theory with specific reaction parameters, *J. Phys. Chem.* 95 (1991) 4618–4627.
- [14] Y.-P. Liu, D.-h. Lu, A. González-Lafont, D. G. Truhlar, B. C. Garrett, Direct dynamics calculation of the kinetic isotope effect for an organic hydrogen-transfer reaction, including corner-cutting tunneling in 21 dimensions, *J. Am. Chem. Soc.* 115 (1993) 7806–7817.
- [15] T. C. Allison, D. G. Truhlar, Testing the accuracy of practical semiclassical methods: Variational transition state

- theory with optimized multidimensional tunneling, in: D.-L. Thompson (Ed.), *Modern methods for multidimensional dynamics computations in chemistry*, World Scientific, Singapore, 1998, pp. 618–712.
- [16] J. Pu, D. G. Truhlar, Validation of variational transition state theory with multidimensional tunneling contributions against accurate quantum mechanical dynamics for $\text{H} + \text{CH}_4 \rightarrow \text{H}_2 + \text{CH}_3$ in an extended temperature interval, *J. Chem. Phys.* 117 (2002) 1479.
- [17] D.-G. Truhlar, J. Gao, M. Garcia-Viloca, C. Alhambra, J. Corchado, M.-L. Sanchez, T. D. Poulsen, Ensemble-averaged variational transition state theory with optimized multidimensional tunneling for enzyme kinetics and other condensed-phase reactions, *Int. J. Quantum Chem.* 100 (2004) 1136–1152.
- [18] H. Eyring, The activated complex in chemical reactions, *J. Chem. Phys.* 3 (2) (1935) 107–115.
- [19] D. G. Truhlar, B. C. Garrett, S. J. Klippenstein, Current status of transition-state theory, *J. Phys. Chem.* 100 (1996) 12771–12800.
- [20] C. Eckart, The penetration of a potential barrier by electrons, *Phys. Rev.* 35 (1930) 1303–1309.
- [21] F. S. Klein, A. Persky, R. E. Weston, Jr., Deuterium-isotope effect in the chlorine exchange between hydrogen chloride and chlorine atoms. A study of models for the tunnel effect, *J. Chem. Phys.* 41 (1964) 1799–1807.
- [22] G. Leroy, M. Sana, A. Tinant, Étude théorique des réactions d'abstraction d'hydrogène $\text{RH} + \text{X} \rightleftharpoons \text{R} + \text{HX}$, avec, $\text{R}, \text{X} = \text{H}, \text{CH}_3, \text{NH}_2, \text{OH}$, et F , *Can. J. Chem.* 63 (1985) 1447–1456.
- [23] W. H. Miller, Tunneling corrections to unimolecular rate constants, with applications to formaldehyde, *J. Am. Chem. Soc.* (1979) 6810–6814.
- [24] D. G. Truhlar, A. Kupperman, Exact tunneling calculations, *J. Am. Chem. Soc.* 93 (1971) 1840–1851.
- [25] B. C. Garrett, D. G. Truhlar, R. S. Grev, A. W. Magnuson, Improved treatment of threshold contributions in variational transition state theory, *J. Phys. Chem.* 84 (1980) 1730–1748.
- [26] B. C. Garrett, D. G. Truhlar, Criterion of minimum state density in the transition state theory of bimolecular reactions, *J. Chem. Phys.* 70 (4) (1979) 1593–1598.
- [27] B. C. Garrett, D. G. Truhlar, Generalized transition state theory. Classical mechanical theory and applications to collinear reactions of hydrogen molecules, *J. Phys. Chem.* 83 (1979) 1052–1078.
- [28] R. T. Skodje, D. G. Truhlar, B. C. Garrett, Vibrationally adiabatic models for reactive tunneling, *J. Chem. Phys.* 77 (1982) 5955–5976.
- [29] D.-h. Lu, T. N. Truong, V. S. Melissas, G. C. Lynch, Y.-P. Liu, B. C. Garrett, R. Steckler, A. D. Isaacson, S. N. Rai, G. C. Hancock, J. G. Lauderdale, T. Joseph, D. G. Truhlar, Polyrate 4: A new version of a computer program for the calculation of chemical reaction rates for polyatomics, *Comput. Phys. Commun.* 71 (1992) 235.
- [30] Y.-P. Liu, G. C. Lynch, T. N. Truong, D.-h. Lu, D. G. Truhlar, Molecular modeling of the kinetic isotope effect for the [1,5]-sigmatropic rearrangement of cis-1,3-pentadiene, *J. Am. Chem. Soc.* 115 (1993) 2408–2415.
- [31] J. Zheng, T. Yu, E. Papajak, I. M. Alecu, S. L. Mielke, D. G. Truhlar, Practical methods for including torsional anharmonicity in thermochemical calculations on complex molecules: The internal-coordinate multi-structural approximation, *Phys. Chem. Chem. Phys.* 13 (2011) 10885–10907.
- [32] T. Yu, J. Zheng, D. G. Truhlar, Multi-structural variational transition state theory. kinetics of the 1,4-hydrogen shift isomerization of the pentyl radical with torsional anharmonicity, *Chem. Sci.* 2 (2011) 2199–2213.
- [33] T. Yu, J. Zheng, D. G. Truhlar, Multipath variational transition state theory: rate constant of the 1,4-hydrogen shift isomerization of the 2-cyclohexylethyl radical, *J. Phys. Chem. A* 116 (2012) 297–308.
- [34] R. Meana-Pañeda, A. Fernández-Ramos, Tunneling and conformational flexibility play critical roles in the isomerization mechanism of vitamin d, *J. Am. Chem. Soc.* 134 (2012) 346–354; (E) 134 (2012) 7193.
- [35] D. Ferro-Costas, M. N. D. S. Cordeiro, D. G. Truhlar, A. Fernández-Ramos, Q2DTor: A program to treat torsional anharmonicity through coupled pair of torsions in flexible molecules, *Comput. Phys. Commun.* 232 (2018) 190–205.
- [36] J. Zheng, S. L. Mielke, K. L. Clarkson, D. G. Truhlar, MSTor: A program for calculating partition functions, free energies, enthalpies, entropies, and heat capacities of complex molecules including torsional anharmonicity, *Comput. Phys. Commun.* 183 (2012) 1803–1812.
- [37] J. Zheng, R. Meana-Pañeda, D. G. Truhlar, MSTor version 2013: A new version of the computer code for the multi-structural torsional anharmonicity, now with a coupled torsional potential, *Comput. Phys. Commun.* 184 (2013) 2032–2033.
- [38] D. T. Gillespie, A general method for numerically simulating the stochastic time evolution of coupled chemical reactions, *J. Comput. Chem.* 22 (1976) 403–434.
- [39] D. T. Gillespie, Stochastic simulation of chemical kinetics, *Annu. Rev. Phys. Chem.* 58 (2007) 35–55.
- [40] D. Ferro-Costas, E. Martínez-Núñez, J. Rodríguez-Otero, E. Cabaleiro-Lago, C. M. Estévez, B. Fernández, A. Fernández-Ramos, S. A. Vázquez, Influence of multiple conformations and paths on rate constants and product branching ratios. thermal decomposition of 1-propanol radicals, *J. Phys. Chem. A* 122 (2018) 4790–4800.
- [41] J. Zheng, J. L. Bao, R. Meana-Pañeda, S. Zhang, B. J. Lynch, J. C. Corchado, Y.-Y. Chuang, P. L. Fast, W.-P. Hu, Y.-P. Liu, G. C. Lynch, K. A. Nguyen, C. F. Jackels, A. Fernández-Ramos, B. A. Ellingson, V. S. Melissas, J. Villà, I. Rossi, E. L. Coitiño, J. Pu, T. V. Albu, A. Ratkiewicz, R. Steckler, B. C. Garrett, A. D. Isaacson, D. G. Truhlar,

- Polyrate–version 2017-C: Computer Program for the Calculation of Chemical Reaction Rates for Polyatomics; University of Minnesota: Minneapolis, 2017.
- [42] W. J. Hehre, R. F. Stewart, J. A. Pople, Self-consistent molecular-orbital methods. i. use of gaussian expansions of slater-type atomic orbitals, *J. Chem. Phys.* 51 (1969) 2657–2664.
- [43] A. Fernández-Ramos, B. A. Ellingson, R. Meana-Pañeda, J. M. C. Marques, D. G. Truhlar, Symmetry numbers and chemical reaction rates, *Theor. Chem. Acc.* 118 (2007) 813–826.
- [44] D. G. Truhlar, Interpretation of ortho-para hydrogen conversion, *J. Chem. Phys.* 65 (1976) 1008–1010.
- [45] G. C. Schatz, A. Kuppermann, Quantum mechanical reactive scattering for three-dimensional atom plus diatom systems. ii. accurate cross sections for $\text{h}+\text{h}_2$, *J. Chem. Phys.* 65 (1976) 4668–4692.
- [46] A. Chakraborty, D. G. Truhlar, J. M. Bowman, S. Carter, Calculation of converged rovibrational energies and partition function for methane using vibrational-rotational configuration interaction, *J. Chem. Phys.* 121 (2004) 2071–2084.
- [47] J. Merrick, D. Moran, L. Radom, An evaluation of harmonic vibrational frequency scale factors, *J. Phys. Chem. A* 111 (2007) 11683–11700.
- [48] I. M. Alecu, J. Zheng, Y. Zhao, D. G. Truhlar, Computational thermochemistry: Scale factor databases and scale factors for vibrational frequencies obtained from electronic model chemistries, *J. Chem. Theory Comput.* 6 (2010) 2872–2887.
- [49] J. Zheng, R. Meana-Pañeda, D. G. Truhlar, Prediction of experimentally unavailable product branching ratios for biofuel combustion: The role of anharmonicity in the reaction of isobutanol with oh, *J. Am. Chem. Soc.* 136 (2014) 5150–5160.
- [50] L. Gao, J. Zheng, A. Fernández-Ramos, D. G. Truhlar, X. Xu, Kinetics of the methanol reaction with oh at interstellar, atmospheric, and combustion temperatures, *J. Am. Chem. Soc.* 140 (2018) 2906–2918.
- [51] A. Fernández-Ramos, Accurate treatment of two-dimensional non-separable hindered internal rotors, *J. Chem. Phys.* 138 (2013) 134112.
- [52] L. Simón-Carballido, J. L. Bao, T. V. Alves, R. Meana-Pañeda, T. D. G., A. Fernández-Ramos, Anharmonicity of coupled torsions: the extended two-dimensional torsion method and its use to assess more approximate methods, *J. Chem. Theory Comput.* 13 (2017) 3478–3492.
- [53] J. Zheng, D. G. Truhlar, Quantum thermochemistry: multistructural method with torsional anharmonicity based on a coupled torsional potential, *J. Chem. Theory Comput.* 9 (2013) 1356–1367.
- [54] K. Fukui, S. Kato, H. Fujimoto, Constituent analysis of the potential gradient along a reaction coordinate. Method and an application to methane + tritium reaction, *J. Am. Chem. Soc.* 97 (1975) 1–7.
- [55] W. H. Miller, N. C. Handy, J. E. Adams, Reaction path hamiltonian for polyatomic molecules, *J. Chem. Phys.* 72 (1980) 99–112.
- [56] V. S. Melissas, D. G. Truhlar, B. C. Garrett, Optimized calculations of reaction paths and reaction-path functions for chemical reactions, *J. Chem. Phys.* 96 (1992) 5758–5772.
- [57] M. Page, J. W. McIver Jr, On evaluating the reaction path Hamiltonian, *J. Chem. Phys.* 88 (1988) 922–935.
- [58] M. Page, Electronic structure computations and theoretical chemical kinetics: developments at the interface, *Comput. Phys. Commun.* 84 (1994) 115–130.
- [59] D. G. Truhlar, A. Kuppermann, Exact and approximate quantum mechanical reaction probabilities and rate constants for the collinear $\text{H}+\text{H}$ reaction, *J. Chem. Phys.* 56 (5) (1972) 2232–2252.
- [60] J. G. Lauderdale, D. G. Truhlar, Diffusion of hydrogen, deuterium, and tritium on the (100) plane of copper: Reaction-path formulation, variational transition state theory, and tunneling calculations, *Surf. Sci.* 164 (1985) 558–588.
- [61] S. E. Wonchoba, D. G. Truhlar, General potential-energy function for H/Ni and dynamics calculations of surface diffusion, bulk diffusion, subsurface-to-surface transport, and absorption, *Phys. Rev. B* 53 (1996) 11222–11241.
- [62] G. A. Natanson, B. C. Garrett, T. N. Truong, T. Joseph, D. G. Truhlar, The definition of reaction coordinates for reaction-path dynamics, *J. Chem. Phys.* 94 (1991) 7875.
- [63] E. B. Wilson, Jr., J. C. Decius, P. C. Cross, *Molecular Vibrations*, Dover Publications, Inc., New York, 1955.
- [64] A. D. Isaacson, D. G. Truhlar, K. Scanlon, J. Overend, Tests of approximation schemes for vibrational energy-levels and partition-functions for triatomics - H_2O and SO_2 , *J. Chem. Phys.* 75 (1981) 3017–3024.
- [65] C. Jackels, Z. Gu, D. G. Truhlar, Reaction-path potential and vibrational frequencies in terms of curvilinear internal coordinates, *J. Chem. Phys.* 102 (1995) 3188–3201.
- [66] K. A. Nguyen, C. F. Jackels, D. G. Truhlar, Reaction-path dynamics in curvilinear internal coordinates including torsions, *J. Chem. Phys.* 104 (1996) 6491–6496.
- [67] Y.-Y. Chuang, D. G. Truhlar, Reaction-path dynamics with harmonic vibration frequencies in curvilinear internal coordinates: $\text{H} + \text{trans-N}_2\text{H}_2 \rightarrow \text{NH}_2 + \text{H}_2$, *J. Chem. Phys.* 107 (1997) 83–89.
- [68] Y. Y. Chuang, D. G. Truhlar, Reaction-path dynamics in redundant internal coordinates, *J. Phys. Chem. A* 102 (1998) 242–247.
- [69] M. A. Pariseau, I. Suzuki, J. Overend, Least-squares adjustment of anharmonic potential constants: Application to

- $^{12}\text{CO}_2$ and $^{13}\text{CO}_2$, *J. Chem. Phys.* 42 (1965) 2335–2344.
- [70] D. F. McIntosh, K. H. Michaelian, M. R. Peterson, A consistent derivation of the Wilson–Decius s vectors, including new out-of-plane wag formulae, *Can. J. Chem.* 56 (1978) 1289–1295.
- [71] M. Challacombe, J. Cioslowski, Coordinate transformations of cubic force constants and transferability of anharmonic force constants in internal coordinates, *J. Chem. Phys.* 95 (1991) 1064–1068.
- [72] P. Pulay, G. Fogarasi, Geometry optimization in redundant internal coordinates, *J. Chem. Phys.* 96 (1992) 2856–2860.
- [73] V. Bakken, T. Helgaker, The efficient optimization of molecular geometries using redundant internal coordinates, *J. Chem. Phys.* 117 (2002) 9160–9174.
- [74] D. McIntosh, The determination of Wilson–Decius f matrix elements from cartesian force constants, *Theor. Chem. Acc.* 125 (2010) 177–184.
- [75] L. Simón-Carballido, T. V. Alves, A. Dybala-Defratyka, A. Fernández-Ramos, Kinetic isotope effects in multipath vtst: Application to a hydrogen abstraction reaction, *J. Chem. Phys.* B 120 (2016) 1911–1918.
- [76] J. Zheng, D. G. Truhlar, Kinetics of hydrogen-transfer isomerizations of butoxyl radicals, *Phys. Chem. Chem. Phys.* 12 (2010) 7782–7793.
- [77] Y.-Y. Chuang, J. C. Corchado, D. G. Truhlar, Mapped interpolation scheme for single-point energy corrections in reaction rate calculations and a critical evaluation of the dual-level reaction path dynamics methods, *J. Phys. Chem. A* 103 (1999) 1140–1149.
- [78] A. Fernández-Ramos, D. G. Truhlar, Improved algorithm for corner-cutting tunneling calculations, *J. Chem. Phys.* 114 (2001) 1491–1496.
- [79] A. Fernández-Ramos, D. G. Truhlar, J. Corchado, J. Espinosa-García, Interpolated algorithm for large-curvature tunneling calculations of transmission coefficients for variational transition state theory calculations of reaction rates, *J. Phys. Chem. A* 106 (2002) 4957–4960.
- [80] A. Fernández-Ramos, D. G. Truhlar, A new algorithm for efficient direct dynamics calculations of large-curvature tunneling and its application to radical reactions with 9–15 atoms, *J. Chem. Theory Comput* 1 (6) (2005) 1063–1078.
- [81] B. C. Garrett, D. G. Truhlar, A least-action variational method for calculating multidimensional tunneling probabilities for chemical reactions, *J. Chem. Phys.* 79 (1983) 4931–4938.
- [82] R. Meana-Pañeda, D. G. Truhlar, A. Fernández-Ramos, Least-action transmission coefficient for polyatomic reactions, *J. Chem. Theory Comput.* 6 (2010) 6–17.
- [83] R. Meana-Pañeda, D. G. Truhlar, A. A. Fernández-Ramos, Direct dynamics implementation of the least-action tunneling transmission coefficient. Application to the $\text{CH}_4/\text{CD}_3\text{H}/\text{CD}_4 + \text{CF}_3$ abstraction reactions, *J. Chem. Theory Comput.* 6 (2010) 3015–3025.